

# Amyloid $\beta$ oligomer selective antibodies for Alzheimer's therapeutics and diagnostics

**Running title: A $\beta$ O-antibodies for therapeutics and diagnostics**

## Authors

Kirsten L. Viola<sup>1\*</sup>, Maira A. Bicca<sup>1</sup>, Adrian M. Bebenek<sup>3</sup>, Daniel L. Kranz<sup>1</sup>, Vikas Nandwana<sup>2</sup>, Emily A. Waters<sup>4</sup>, Chad R. Haney<sup>4</sup>, Maxwell Lee<sup>1</sup>, Abhay Gupta<sup>3</sup>, Zach Brahmhatt<sup>3</sup>, Weijian Huang<sup>1</sup>, Ting-Tung Chang<sup>5,6</sup>, Anderson Peck<sup>5,6</sup>, Clarissa Valdez<sup>1</sup>, Vinayak P. David<sup>2</sup>, and William L. Klein<sup>1,7</sup>

<sup>1</sup> Northwestern University, Department of Neurobiology, Evanston, IL 60208

<sup>2</sup> Northwestern University, Department of Material Science and Engineering, Evanston, IL 60208

<sup>3</sup> Illinois Math and Science Academy, Aurora, IL 60506

<sup>4</sup> Northwestern University, Center for Advanced Molecular Imaging, Evanston, IL 60208

<sup>5</sup> Van Andel Research Institute, Small Animal Imaging Facility, Grand Rapids, MI 49503

<sup>6</sup> Van Andel Research Institute, Laboratory of Translational Imaging, Grand Rapids, MI 49503

<sup>7</sup> Northwestern University, Department of Neurology, Chicago, IL 60611

\*corresponding author [k-viola@northwestern.edu](mailto:k-viola@northwestern.edu)

Abbreviations: AD-Alzheimer's disease; A $\beta$ O-Amyloid  $\beta$  oligomer; CSF-cerebrospinal fluid; GFAP-glia fibrillar acidic protein; ICV-intracerebroventricular; MNS-magnetic nanostructures; MRI-magnetic resonance imaging; PET-positron emission tomography; NOR-novel object recognition; NLR-novel location recognition; PiB-Pittsburgh Compound B; pTau-phosphorylated tau; ThioS-thioflavin S; Tg-transgenic; WT-wild-type

25

## Abstract

26

27

28

29

30

31

32

33

34

35

36

37

38

39

40

41

42

43

44

45

46

47

48

Improvements have been made in the diagnosis of Alzheimer's disease (AD), manifesting mostly in the development of *in vivo* imaging methods that allow for the detection of pathological changes in AD by MRI and PET scans. Many of these imaging methods, however, use agents that probe amyloid fibrils and plaques- species that do not correlate well with disease progression and are not present at the earliest stages of the disease. Amyloid  $\beta$  oligomers (A $\beta$ O), rather, are now widely accepted as the A $\beta$  species most germane to AD onset and progression. Here we report evidence further supporting the role of A $\beta$ O as pathological instigators of AD and introduce a promising anti-A $\beta$ O diagnostic probe capable of distinguishing the 5xFAD mouse model from wild type mice by PET and MRI. In a developmental study, A $\beta$  oligomers in 5xFAD mice were found to appear at 3 months of age, just prior to the onset of memory dysfunction, and spread as memory worsened. The increase is prominent in the subiculum and correlates with concomitant development of reactive astrocytosis. The impact of these A $\beta$ O on memory is in harmony with findings that intraventricular injection of synthetic A $\beta$ O into wild type mice induced hippocampal dependent memory dysfunction within 24 hours. Compelling support for the conclusion that endogenous A $\beta$ O cause memory loss was found in experiments showing that intranasal inoculation of A $\beta$ O-selective antibodies into 5xFAD mice completely restored memory function, measured 30 days post-inoculation. These antibodies, which were modified to give MRI and PET imaging probes, were able to distinguish 5xFAD mice from wild type littermates. These results provide strong support for the role of A $\beta$ O in instigating memory loss and salient AD neuropathology, and they demonstrate that A $\beta$ O selective antibodies have potential both for therapeutics and for diagnostics.

KEYWORDS: A $\beta$  oligomers; Alzheimer's disease; 5xFAD; MRI; PET; diagnostics; therapeutics

49

## Introduction

50

### General Alzheimer's disease

51 More than 6 million Americans are currently living with Alzheimer's disease (AD), and Alzheimer's-related  
52 deaths have increased 145% from 2000 to 2019 (2021). The financial burden is even more staggering-  
53 Alzheimer's and other dementias have cost the US more than \$600 billion in medical expenses and  
54 unpaid care in 2021 (2021). Despite the great personal and economic burden, progress toward  
55 developing effective diagnostics and therapeutics remains slow. Aduhelm® (also known as  
56 Aducanumab) was recently approved as a treatment for Alzheimer's disease (Investor Relations, 2021),  
57 the first in more than a decade, but it still focuses on A $\beta$  elimination rather than specific A $\beta$ O targets. As  
58 AD burden is expected to increase drastically with the aging population, improved diagnostics and  
59 therapeutics are more urgent now than ever.

60

### A $\beta$ O<sub>s</sub> as a biomarker for early Alzheimer's disease

61 The primary pathological hallmarks of Alzheimer's disease are extracellular amyloid plaques and  
62 intraneuronal tangles of hyperphosphorylated tau (Masters et al., 1985). It is well known, however, that  
63 amyloid plaques do not correlate well with cognitive decline in AD (Terry et al., 1991; Hsia et al., 1999;  
64 Lee et al., 2004) and are not present in the earliest stages of the disease (Nyborg et al., 2013). Research  
65 from the previous two decades strongly indicates that soluble amyloid beta oligomers (A $\beta$ O<sub>s</sub>), not  
66 plaques, are the more appropriate amyloid beta species to target in AD (Ashe, 2020; Hampel et al., 2021).

67 A $\beta$ O<sub>s</sub> are potent neurotoxins that show AD-dependent accumulation in the brain of AD patients (Gong et al.,  
68 2003; Kaye et al., 2003; Lacor et al., 2004) and transgenic (Tg) rodent AD models (Chang et al.,  
69 2003; Lesne et al., 2006; Ohno et al., 2006). For reviews of other perspectives regarding AD molecular  
70 etiology, see (Braak and Del Tredici, 2011; Robakis, 2011; Lasagna-Reeves et al., 2012). A $\beta$ O<sub>s</sub> begin to  
71 accumulate early in AD, decades prior to symptoms, and are widely held to be the neurotoxic instigators  
72 of AD (Rodgers, 2005; Gandy et al., 2010; Schnabel, 2011; Mucke and Selkoe, 2012). A $\beta$ O<sub>s</sub> have been  
73 shown to exert their toxic effects by instigating failure of synaptic plasticity and memory (Lambert et al.,  
74 1998; Wang et al., 2002; Lesne et al., 2006; Townsend et al., 2006). Recently, soluble cortical extracts  
75 were examined by ELISA and showed that the ratio of A $\beta$ O levels to plaque density fully distinguished  
76 demented from non-demented patients (Esparza et al., 2013); simply put, those with high A $\beta$ O to plaque  
77 ratios were demented and low A $\beta$ O to plaque ratios were not.

78

### The 5xFAD mouse model

79 The 5xFAD transgenic mice is an increasingly used AD model that harbors gene mutations in amyloid  $\beta$   
80 protein precursor (A $\beta$ PP) (K670N/M671L + I716V + V717I) and presenilins (PS1/2) (M146L + L286V)  
81 (Oakley et al., 2006). These mutations are known to increase production of A $\beta$ 42, characteristic of familial  
82 AD, and exhibit expedited plaque development compared to other transgenic mice (Oakley et al., 2006).  
83 The Mutant Mouse Resource Research Center (MMRRC) found that A $\beta$  accumulation occurred at  
84 different rates, depending on the breeding background, with mice bred on a B6SJL background  
85 developing pathology at a significantly more rapid rate (unpublished, available at [MMRRC 5xFAD strain data](#))  
86 than those bred on a C57 background. The 5xFAD mouse model is well characterized for memory  
87 impairments (Oakley et al., 2006; Kimura and Ohno, 2009; Ohno, 2009; Girard et al., 2013; Girard et al.,  
88 2014; Zhang et al., 2021a), neuron loss (Jawhar et al., 2012; Oblak et al., 2021), and A $\beta$  plaque  
89 accumulation (Devi et al., 2010; Jawhar et al., 2012; Ashe, 2020; Zhang et al., 2021a). Comprehensive  
90 studies on the 5xFAD model have also looked at cholesterol and glucose levels (Oblak et al., 2021),  
91 activity levels (Oblak et al., 2021), neuroinflammation-related protein levels (Ou-Yang and Van Nostrand,  
92 2013; Oblak et al., 2021), tau phosphorylation (Shao et al., 2011; Kanno et al., 2014), and visual acuity  
93 (Zhang et al., 2021a).

94

### Alzheimer's disease diagnostics

95 Recommended tests ([Alzheimer's Disease Diagnostic Guidelines | National Institute on Aging \(nih.gov\)](#))  
96 for diagnosing Alzheimer's disease include a standard health evaluation and MMSE evaluations. If  
97 indicated, these tests are typically followed with cerebrospinal fluid (CSF) assays for tau and A $\beta$  levels,  
98 MRI for brain volume and functionality, and positron emission tomography (PET) scans for A $\beta$  plaques,  
99 glucose metabolism, and/or tau fibrils in the brain (Albert et al., 2011; Jack et al., 2011; McKhann et al.,  
100 2011; Sperling et al., 2011). These analyses may rule out other dementia etiologies and help to determine  
101 disease severity, but they cannot detect AD at its earliest stages or closely predict disease progression,  
102 as they do not probe for AD's earliest biomarkers.

### 103 **Current diagnostic methods in development**

104 Spinal taps are invasive, but cerebrospinal fluid assays show promise (Georganopoulou et al., 2005;  
105 Toledo et al., 2013b). Nonetheless, assays using CSF analytes have presented challenges with respect  
106 to accuracy and reliable disease-state discrimination (Slemmon et al., 2012). More recently, assays for  
107 A $\beta$ O levels in the blood plasma have been developed with promising results (Meng et al., 2019). These  
108 assays show a correlation between A $\beta$ O levels and declining memory scores that appear not to be  
109 influenced by age, gender, or ApoE4 status. A promising addition to diagnostic methodology is the  
110 detection of AD pathology using targeted *in vivo* brain imaging. The introduction of PET probes for  
111 amyloid plaques has been a great technical advance (Klunk et al., 2004) and has established precedent  
112 for the usefulness of brain molecular imaging as a diagnostic tool and for proof of efficacy in drug  
113 development (Johnson et al., 2013). Still, these new imaging tools focus on late-stage AD pathology, not  
114 on the early biomarkers such as A $\beta$ O.

115 Prior studies using 5xFAD mice have examined early and late-stage disease development, but none  
116 have looked at the progressive development of A $\beta$ O in this model. Here, we present an analysis of  
117 memory impairment from 2-9 months of age and the progressive accumulation of A $\beta$ O across the same  
118 age-span. Our studies presented here use an A $\beta$ O-selective antibody to characterize the spatiotemporal  
119 development of A $\beta$ O in the 5xFAD mouse model and demonstrate a correlation with memory  
120 impairment. Strikingly, intranasal inoculation of the A $\beta$ O-selective antibody rescued memory performance  
121 in 6-month-old 5xFAD mice. We demonstrate the capability of detecting A $\beta$ O pathology *in vivo* in the  
122 5xFAD mouse by introducing molecular imaging modalities (MRI and PET) with probes for A $\beta$ O. We  
123 additionally present immunofluorescent evidence of a remarkable association between A $\beta$ O and GFAP-  
124 positive reactive astrocytes in the 5xFAD mice. Taken together, we provide further data implicating A $\beta$ O  
125 as essential diagnostic indicators and therapeutic targets, and show evidence suggesting a mechanism  
126 through which A $\beta$ O instigate pathological abnormalities: by induction of reactive astrogliosis.

127

128

## Materials and Methods

### 129 Materials

130 ACU193 humanized anti-A $\beta$ O antibody was a generous gift from Acumen Pharmaceuticals, Inc. A $\beta$ <sub>1-42</sub>  
131 (TFA preparation) was sourced from multiple suppliers. Primary hippocampal cultures were prepared  
132 from tissue obtained from BrainBits, LLC, using media and reagents also obtained from BrainBits. All  
133 chemicals were purchased from Sigma unless otherwise specified.

### 134 Animals

135 5x*FAD* Tg mouse model (B6SJL-Tg(APP<sup>S</sup>W<sup>FIL</sup>on,PSEN1\*<sup>M146L</sup>\*L286V)<sup>6799Vas</sup>)(Oakley et al., 2006)  
136 (Jackson Laboratories) was bred on a non-transgenic background (B6SJL<sup>F1/J</sup> mice (Jackson  
137 Laboratories, RRID: IMSR\_JAX:100012)). Aged transgenic and wild-type littermates, 2-20 months old,  
138 were used. All mice were kept under a 12/12 h light/dark cycle (7 AM/7 PM) at 22  $\pm$  2 °C. Mice had free  
139 access to food and water, including during behavioral experiments, were housed at  $\leq$ 5/cage (NexGen  
140 IVC, Allentown) with enriched environment and daily veterinarian assessment, according to NU's  
141 standard procedures. Procedures complied with NIH's Guide for the Care and Use of Laboratory Animals  
142 (NIH publication No. 80-23, 1996) and were approved by IACUC (protocol #IS00004010). Behavioral  
143 experiments were conducted between 12-6 PM.

144 For intracerebroventricular (icv) experiments, B6SJL<sup>F1/J</sup> mice (Jackson Laboratories, RRID:  
145 IMSR\_JAX:100012) were utilized at ages ranging from 6 months of age (30-50 g).

### 146 A $\beta$ Oligomer Preparation

147 Fluorescently-labeled A $\beta$  oligomers were prepared essentially according to the protocol published by  
148 Klein and colleagues.(Lambert et al., 2007) Briefly, A $\beta$ <sub>1-42</sub> (American Peptide or Peptides International)  
149 or FAM-A $\beta$ <sub>1-42</sub> (Anaspec) was dissolved in hexafluoro-2-propanol (HFIP) and distributed into  
150 microcentrifuge tubes. Hexafluoro-2-propanol was removed by evaporation and traces removed under  
151 vacuum; the tubes were stored at -80°C. An aliquot of each was dissolved in anhydrous dimethyl sulfoxide  
152 (DMSO) to ~5 mM, mixed 5:1 (mol: mol) A $\beta$ : FAM-A $\beta$ , and diluted in ice-cold Ham's F12 medium without  
153 phenol red (Caisson Laboratories) to 100  $\mu$ M. This solution was incubated at 4°C for 24 hr. and  
154 centrifuged at 14 000 g for 10 min. The supernatant, defined as the FAM-A $\beta$ O preparation, was  
155 transferred to a clean microfuge tube and stored at 4°C until use. Protein concentration was determined  
156 using Coomassie Plus protein assay kit (Pierce).

157 The same protocol was employed to prepare unlabeled A $\beta$  oligomers in the absence of FAM-A $\beta$ <sub>1-42</sub>. A  
158 modification of this protocol was used to produce crosslinked A $\beta$ O<sub>s</sub> (Cline et al., 2019b).

### 159 Cell Culture

160 Hippocampal cells were prepared and maintained for at least 18 days as previously described (Gong et  
161 al., 2003) by using (0.002%) poly-L-lysine coated coverslips plated at a density of 1.04 x 10<sup>4</sup> cells per  
162 cm<sup>2</sup> in Neurobasal media (Brainbits, LLC) with B27 supplements and L-glutamine (2.5  $\mu$ M).

### 163 A $\beta$ Oligomer Incubation and Immunolabeling of Cells

164 Cells were incubated at 37°C in conditioned media collected from the cell cultures containing crosslinked  
165 A $\beta$ O<sub>s</sub> or FAM-A $\beta$ O<sub>s</sub> or an equivalent dilution of vehicle. Following incubation with A $\beta$ O<sub>s</sub> or vehicle for 60  
166 min, the cells were rinsed rapidly 3 times with warm media then fixed by adding an equal volume of warm  
167 3.7% formaldehyde (in PBS) to the third rinse in each well/dish and allowing it to sit at RT for 5 min. The  
168 media/formaldehyde was completely removed and replaced with a volume of 3.7% formaldehyde for 5  
169 min at RT. Cells were blocked in 10% normal goat serum (NGS) in PBS or HBSS for 45 min at RT then  
170 incubated overnight at 4°C on an orbital shaker with fluorescent-tagged antibody or anti-A $\beta$ O probe  
171 diluted in blocking buffer. The cells were washed 3 times for 5 min each with PBS or HBSS. After



172 secondary antibody incubation, coverslips were mounted onto glass slides using ProLong Gold Anti-fade  
173 reagent with DAPI (Invitrogen) and imaged using an epifluorescence (TE2000, Nikon), a widefield  
174 fluorescence microscope (Leica DM6B, Leica Corp.), or confocal microscope (Leica SP2, Leica Corp).

### 175 **A $\beta$ O intracerebroventricular (icv) administration in mice**

176 Icv injections and behavior testing were performed in 4 independent experiments of 13-21 mice each.  
177 Littermates were arbitrarily assigned to different injection groups, targeting 5-10 mice/group for statistical  
178 power ( $n = ((Z_{\alpha/2} * \sigma) / E)^2$  at  $\alpha = 0.05$ ;  $\sigma = 10.55$  and  $E = 6.67$  derived from pilot studies).

179 Mice were lightly anesthetized (2% isoflurane) during injection (~1 min). A $\beta$ O<sub>s</sub> (1, 10 pmol in 3  $\mu$ l) or  
180 vehicles were administered icv free-handed (Bicca et al., 2015). Separate needles were used for each  
181 vehicle, progressing from low-high A $\beta$ O concentration to minimize carryover. No analgesics or anti-  
182 inflammatory agents were necessary. Mice were monitored constantly for recovery of consciousness and  
183 ambulation, then periodically for food-and-water intake until behavior analysis. Needle placement was  
184 confirmed by brain dissection after behavioral experiments (euthanization: CO<sub>2</sub> then decapitation). Mice  
185 showing needle misplacement (3 mice) or cerebral hemorrhage (2 mice) were excluded from analysis;  
186 final n = 5-7 mice/group.

### 187 **Object Recognition/Location Recognition (NOR/NLR) Tasks**

188 Tasks were performed essentially as described (Bicca et al., 2015), to evaluate mouse ability to  
189 discriminate between familiar and new, or displaced, objects within an area, measured by object  
190 exploration (sniffing, touching). The open-field testing arena was constructed of gray polyvinyl chloride at  
191 21x21x12" (WxLxH), with a 5x5 square grid on floor and visual cue on wall. 24 h post-injection, mice  
192 underwent 6 min sessions of habituation and training, with 3 min between. All sessions were video  
193 recorded and analyzed by two researchers blind to experimental groups. During habituation and training,  
194 mice were screened for ability to move about the arena and explore the objects, two activities required  
195 for accurate memory assessment in subsequent testing sessions. Locomotive inclusion criteria (>100  
196 grid crossings and >15 rearings; evaluated in habituation) were based on extensive previous experiments  
197 with the same mouse strain and arena; 3/65 mice did not meet this criterion. During training, mice were  
198 placed at the arena center with two objects, which were plastic and varied in shape, color, size and  
199 texture. Exploration inclusion criteria were low exploration (<3 sec total) or object preference (>50% of  
200 total time for either object); 7 of remaining 62 mice did not meet this criterion.

201 Hippocampal-related memory function was assessed 24 h post-training by displacing one of the two  
202 training objects. Cortical-related memory function was assessed 24 h later by replacing the displaced  
203 object with a novel object. Hippocampal-related memory function was re-tested 31-38 days post-injection  
204 by displacing the novel object. Memory dysfunction was defined as an exploration of the familiar object  
205 for >40% total time. Mice were arbitrarily assessed by cage. The arena and objects were cleaned  
206 thoroughly between sessions with 20% (v/v) alcohol to minimize olfactory cues.

### 207 **Immunolabeling of slices**

208 Free floating 45  $\mu$ m thick sagittal sections were cut using a Leica SM2010 R sliding microtome and  
209 transferred to sterile TBS for storage. Sections were gathered and placed sequentially into wells (~4 per  
210 well). Sections were then randomly selected from each well to perform antibody staining using the primary  
211 antibodies ACU193 (0.2  $\mu$ g/ml), Alexa Fluor® 555-conjugated NU4 (0.92  $\mu$ g/ml), Cy3-conjugated anti-  
212 GFAP (1:800, Sigma) and the secondary antibody Alexa Fluor® 633 goat anti-human IgG (1:2000,  
213 Invitrogen). Floating slices were rinsed 3x10 min with TBS and blocked with blocking buffer (10% NGS  
214 with 0.3% Triton X-100 in TBS) for 60 min at room temperature. Slices were then incubated with the  
215 respective antibodies in blocking buffer overnight at 4°C with gentle rotation. Sections were washed 3 x  
216 10 mins in TBS and incubated with secondary antibody for 3 hours at room temperature (RT) with orbital  
217 agitation in the dark. Secondary was prepared in blocking buffer diluted 10-fold with TBS. Sections were  
218 then washed 3 x 10 mins in TBS, mounted using ProLong Diamond® antifade mounting media with DAPI

219 (Invitrogen) and 24x60mm No.1.5 glass coverslips (Thermo Scientific). Z-stacks of the brain sections  
220 were collected at 10x or 100x on a Leica SP5 confocal microscope and analyzed with ImageJ.

221

## 222 **Thioflavin S counterstain.**

223 Thioflavin-S counterstaining to NU4 immunofluorescence labeling was performed as previously  
224 described (Guntern et al., 1992) with a few modifications (Viola et al., 2015). 5xFAD and WT brains were  
225 sliced at a thickness of 50 $\mu$ m and immunolabeled following the same protocol described above  
226 (immunolabeling of slices). Slices were incubated with antibody as described above. The slices were  
227 then washed with PBS for 5 times 5 min each and incubated with 0.002% of Thioflavin-S solution in TBS-  
228 T (diluted from a stock solution 0.02% of Thioflavin-S in distilled water) for 10min. Slices were then  
229 washed 3 times for 1 min in 50% ethanol and 2 times in TBS-T for 5 min. The slices were mounted with  
230 ProLong Gold Antifade reagent for examination by fluorescence microscopy. Images were acquired at  
231 40x magnification and analyzed by ImageJ software.

## 232 **Radiolabeling and Quality Control**

233 Antibodies, NU4 and non-specific mouse IgG or ACU193 and non-specific human IgG were radiolabeled  
234 with positron emitter  $^{64}\text{Cu}$  ( $^{64}\text{CuCl}_2$  in 0.1 M HCl; radionuclide purity >99%, Washington University). For  
235 radiolabeling, Wipke and Wang's method was applied (Wipke et al., 2002). Basically, antibodies  
236 mentioned above were conjugated with DOTA-NHS-ester (Macrocyclics, Dallas, TX) and then  
237 radiolabeled with  $^{64}\text{Cu}$ .

### 238 **Conjugation.**

239 Antibody solutions were buffer exchanged with PBS using YM-30 Centricon® centrifugal filters (Millipore,  
240 Billerica, MA). For conjugation, antibodies were reacted with DOTA-NHS-ester in 0.1 M  $\text{Na}_2\text{HPO}_4$  buffer  
241 of pH 7.5 at 4°C for 12 - 16 h in a molar ratio of DOTA-NHS-ester:antibody = 100: 1. After conjugation,  
242 the reaction mixture was centrifuged repeatedly (5 times) through a YM-30 Centricon® centrifugal filter  
243 with 0.1M pH 6.5 ammonium citrate buffer to remove unconjugated small molecules. The concentrations  
244 of purified antibody-conjugate was determined by measuring the absorbance at 280 nm in a UV  
245 spectrophotometer.

### 246 **Labeling.**

247 When labeling with  $^{64}\text{Cu}$ , 1 mg DOTA-conjugated NU4 and 5 mCi (185 MBq) of  $^{64}\text{Cu}$  as incubated in 0.1  
248 M ammonium citrate buffer, pH 6.5, at 43°C for 1 hour. Labeled antibody was separated by a size-  
249 exclusion column (Bio-Spin6, BIO-RAD Laboratories).

### 250 **Quality Control.**

251 Radiochemical purity of antibody was determined by integrating areas on the Fast Protein Liquid  
252 Chromatography (FPLC) equipped with a flow scintillation analyzer. This analysis was conducted on a  
253 superpose 12 size-exclusion column and characterized by the percentage of radioactivity associated with  
254 the 150 kDa protein peak. The stability of the  $^{64}\text{Cu}$  radiolabeled mAbs was determined by bovine serum  
255 challenge at 44 hours.

### 256 **Conjugation efficiency.**

257 Based on our preliminary data, > 90% of conjugation rate, >70% of labeling rate is achieved by following  
258 prescribed protocol.

## 259 **Overall details of micro PET and micro CT acquisition**

260 Mice were placed in a 37.5 °C heated cage 20-30 minutes prior to radiotracer injection and moved to a  
261 37.5 °C heated induction chamber 10 minutes prior to injection where they were anesthetized with 2-3%  
262 isoflurane in 1000 cc/min  $\text{O}_2$ . A dose of 40  $\mu\text{g}/200 \mu\text{Ci}$  in 100  $\mu\text{L}$  of proposed PET tracers was  
263 administered intravenously through the tail vein. Each animal was administered a dose ranging from 30-

264 40 µg NU4PET, ACU193PET, or non-immune IgGPET. Probes were administered in a single dose.  
265 PET/CT imaging was conducted at 0, 4, 24, and 48 h to measure for changes in distribution and time  
266 required for probe clearance or decay.

267 NU4PET scans were acquired using a Genisys<sup>4</sup> PET (Sofie Biosciences, Culver City, CA) system and  
268 CT scans were acquired using a Bioscan NanoSPECT/CT (Washington, D.C.). When scanning, all mice  
269 were placed prone on the bed of the scanner. A 10 minute static acquisition was used for PET imaging  
270 followed immediately by a 6.5 minute CT acquisition both utilizing the mouse imaging chamber from the  
271 Genisys<sup>4</sup>. PET reconstruction was performed without attenuation correction using 3D Maximum  
272 Likelihood Expectation Maximization (MLEM) with 60 iterations and CT reconstruction used Filtered Back  
273 Projection with a Shepp-Logan Filter. PET and CT reconstructions were exported in dicom image format  
274 and fused using custom software developed by the Small Animal Imaging Facility at Van Andel Institute.  
275 Fused PET/CT images were analyzed using VivoQuant Image Analysis Suite (inviCRO, LLC, Boston,  
276 MA). Standardized Uptake Values (SUV) were calculated using the mouse body weight and corrected  
277 for residual dose in the injection syringe and the injection site, as applicable. The formula used to  
278 calculate SUV was

$$279 \quad SUV = \frac{\text{Activity}_{\text{tissue}}/\text{Volume}_{\text{tissue}}}{\text{Injected Activity}/\text{BodyWeight}}$$

## 280 Evaluation NU4PET (<sup>64</sup>Cu-NU4) in AβOs detection

281 2 groups (n = 3/ group) of 6 months old 5xFAD Tg AD mouse model and 2 groups (n = 3/ group) WT  
282 mouse model were used for evaluating the capability of AβOs detection. NU4PET (<sup>64</sup>Cu-NU4) or non-  
283 specific IgGPET (<sup>64</sup>Cu-IgG) was injected into each 5xFAD Tg AD mouse model and WT mouse model  
284 groups, respectively.

285 Target (AβOs)–Background (normal tissue) contrasts in PET images were used to distinguish the  
286 difference of the capability of AβOs detection between NU4PET and IgGPET in different mouse models.  
287 Tracer uptake of high intensity (hot) areas and background tissues in the brain were chosen by drawing  
288 regions-of-interest (ROI) along the edges of the areas from the PET images. Average pixel values of  
289 each ROIs were acquired and use in Target (AβOs)–Background (normal tissue) contrasts calculation.  
290 The formula used to calculate Target-Background contrast was

$$291 \quad T - B \text{ Contrast} = \frac{\text{Target}_{\text{Average Pixel Value}}}{\text{Background}_{\text{Average Pixel Value}}}$$

## 292 Tissue Biodistribution Assessment

293 Animals were sacrificed immediately after the 44 hour post injection image was acquired. Blood was  
294 collected, while brains and 13 other organs and tissues were harvested and weighed. After the blood  
295 sample was taken from the heart (~500-1000µl), 10 ml of saline was injected into left ventricle while the  
296 heart was still beating to flush out the residual blood in the organs. Radioactivity in each tissue (cpm) wa  
297 measured using the γ-scintillation counter. Percentages of the injected dose/gram (%ID/g) were  
298 calculated for each tissue/ organ by the following formula.

$$299 \quad \%ID/g = \frac{(\text{Sample Activity} - \text{Background})}{(\text{Injected Activity} - \text{Background})(\text{Sample weight}(g))} \times 100\%$$

300 Student's t-test was conducted to the results between different groups.  $P < 0.05$  is considered statistically  
301 significant.

## 302 Synthesis of Magnetic Nanostructures (MNS)

303 16 nm magnetite nanoparticles were synthesized by decomposition of iron-oleate at 320°C as described  
304 in an earlier report.(Park et al., 2004)

305 *Synthesis of Iron-oleate complexes:* 10.8 g of iron (III) chloride hexahydrate and 36.5 g sodium oleate  
306 were dissolved in a mixture of 60 ml distilled water, 80 ml ethanol and 140 ml hexane and heated at 60°C



307 for 4 hr. The organic layer of the biphasic mixture becomes dark, indicating phase transfer of iron (III)  
308 ions and formation of iron oleate complex. The resulting dark solution is separated and washed with water  
309 three times.

310 *Synthesis of 16 nm magnetite nanoparticles:* 18 g of iron oleate complex and 2.58 g of oleic acid were  
311 dissolved in 100 g of octadecene at room temperature and heated to 320°C at a rate of 3.3°C per minute.  
312 The reaction mixture is kept at 320°C for 40 min., then cooled down to room temperature. Resulting  
313 nanoparticles are separated from the solution by addition of ethanol and ethyl acetate followed by  
314 centrifugation.

### 315 **Preparation of Dopamine-TEG-COOH and Phase Transfer**

316 To make the organic phase synthesized MNS suitable for biological application, we functionalized the  
317 MNS using an in-house synthesized ligand with carboxylate as terminal group (for antibody conjugation),  
318 tetraethylene glycol(TEG) as a stabilizer, and nitrodopamine (nDOPA) as an anchor due to its high affinity  
319 for Fe (Nandwana et al., 2016).

320 Synthesis of carboxylate terminated nDOPA ligand and functionalization of the MNS was carried out  
321 according to the following protocol. Tetraethylene diacide, N-hydroxysuccinimide (NHS), N,N'-  
322 Dicyclohexylcarbodiimide (DCC), nDOPA hydrochloride and anhydrous sodium bicarbonate was  
323 dissolved in chloroform under argon atmosphere and stirred for 4 hr. Hexane stabilized MNS were added  
324 and stirred for another 24 hr. The precipitate formed was separated by magnet, dispersed in water and  
325 purified by dialysis.

### 326 **Conjugation of antibody to MNS**

327 The conjugation of buffer stabilized MNS with antibody was done using a conventional carboxyl-amine  
328 crosslinking method. We first activated the carboxyl terminated MNS by sulfo-N-hydroxy succinimide  
329 (SNHS) and 1-Ethyl-3-(3-dimethylaminopropyl)carbodiimide (EDC) followed by incubation with  
330 corresponding antibody (NU4 or IgG<sub>1</sub>, with or without fluorescent label) overnight. Conjugated MNS were  
331 separated by magnet to remove excess reagent and antibody then re-dispersed in working media.  
332 Conjugation efficiency was estimated using UV spectroscopy (absorbance at 280nm) of the magnetically  
333 separated supernatant.

334 Ab conc. = (total mg added Ab) - (mg Ab in supernatant)

### 335 **Intranasal immunization.**

336 Mice were anesthetized with isoflurane and then placed on their backs with their heads positioned to  
337 maximize the residency time for the delivered material to remain on the olfactory surface. Each naris was  
338 administered with ACUMNS or non-immune IgGMNS (10 µl/naris), using a sterile micropipette, slowly  
339 over a period of 1 min, keeping the opposite naris and mouth closed to allow complete aspiration of  
340 delivered material. Steps were repeated up to 5 times, maintaining anesthetization in between  
341 inoculations, for maximum doses of up to 50µl/naris

### 342 **Magnetic Resonance Imaging of Tg and WT mice in vivo**

343 Following intranasal inoculation, the probe was allowed to distribute for 4 hours before MR imaging was  
344 performed according to imaging methodology described in Mundt et al.(Mundt et al., 2009) T1, T2, and  
345 T2\* weighted MR images were acquired on a Bruker BioSpec 9.4T magnet, using a 25 mm RF quadrature  
346 coil. The in-plane resolution was 75 µm with slice thickness 0.4 mm. T1- and T2-weighted images provide  
347 anatomical guidance as well as some localization of the ACUMNS and were acquired with a fat  
348 suppressed spin echo sequence (Rapid Acquisition with Relaxation Enhancement, RARE) with the  
349 following parameters for T1-weighted (TR=1000 ms, TE<sub>eff</sub>=13.2 ms, rare factor 2, number of excitations,  
350 NEX=4) and for T2-weighted (TR=3500 ms, TE<sub>eff</sub>=58.5 ms, rare factor 4, NEX=4). T2\*-weighted imaging  
351 provides more of the localization of the NU4MNS as the iron causes local changes in magnetic  
352 susceptibility which T2\* weighted images can be sensitive to. A gradient echo sequence was used with

353 the following parameters (gradient echo fast imaging, GEFI; TR=1200 ms, TE=5.6 ms, flip angle 35° and  
354 NEX=4).  
355

356

## Results

357

### Memory dysfunction in 5xFAD mice begins shortly after A $\beta$ O emergence and progressively worsens with concomitant A $\beta$ O accumulation in the hippocampus

358

359

#### Tg 5xFAD NOR/NLR

360

361

362

363

364

365

366

367

368

369

370

371

372

373

374

375

376

377

378

379

Amyloid plaque development and intraneuronal A $\beta$ 42 accumulation are well-established in the 5xFAD transgenic (Tg) mouse model of Alzheimer's disease. There is robust plaque buildup around 5-6 months of age (Ohno et al., 2006) and intraneuronal A $\beta$ 42 accumulation begins as early as 2 months (Oakley et al., 2006). The majority of neuropathological studies in 5xFAD mice have used probes that show amyloid plaque development; how 5xFAD memory impairment coincides with A $\beta$ O pathology and development is much less well-characterized. In order to characterize how memory loss correlates with A $\beta$ O in the 5xFAD mice, we used the well-established novel object recognition task (NOR) for non-spatial (cortical) memory (Cohen and Stackman, 2015; Denninger et al., 2018) and the novel location recognition task (NLR) for spatial (hippocampal) memory (Antunes and Biala, 2012; Bengoetxea et al., 2015; Grayson et al., 2015; Denninger et al., 2018). We assessed memory in mice aged 2-18 months. 5xFAD mice showed no evident memory impairment at 2 to 3 months old (Figure 1a). By 4 to 5 months old, most transgenic mice showed memory impairment, and by 6 to 7 months of age memory impairment was apparent in all 5xFAD mice. Importantly, at 4 months old, the majority of 5xFAD mice were impaired in both the hippocampal-dependent and cortical-dependent tasks; there were, however, some mice that showed only cortical-impairment. Though less obvious than their Tg littermates, memory loss was detected at 9 months of age in wild-type mice. In summary, we showed that 5xFAD mice first present memory impairment between 3 and 4 months of age. This memory dysfunction afflicts more mice as their age increases until, at 6 to 7 months, all of the Tg mice are impaired in both hippocampal-dependent and cortical-dependent tasks. These data indicate that memory impairment begins before observed amyloid plaque build-up in the 5xFAD mice.

380

#### Immunohistofluorescence validation of A $\beta$ O development

381

382

383

384

385

386

387

388

389

390

391

392

393

394

395

The development of amyloid plaque pathology is well-established in the 5xFAD mouse model (Oakley et al., 2006; Ohno et al., 2006). Amyloid plaques, however, are no longer considered the most germane A $\beta$  species to AD pathology (Overk and Masliah, 2014; Viola and Klein, 2015; Selkoe and Hardy, 2016; Cline et al., 2018; Li and Selkoe, 2020). Characterizing the development of the most relevant species, putatively A $\beta$ O, and their association with other pathological changes in AD, such as glial activation or pTau accumulation, is necessary to better understand disease progression in this model. Sagittal sections of brain tissue, collected and fixed from WT and 5xFAD mice at ages 2, 3, 4, 6, and 8 months of age, were immunolabeled with ACU193 and imaged using confocal microscopy. ACU193, a humanized monoclonal antibody that targets A $\beta$ O, has been shown to selectively bind oligomers *in vitro* (Krafft et al., 2013; Goure et al., 2014; Savage et al., 2014) and in the TG2576 mouse model. Here, using ACU193 to probe for A $\beta$ O, we show the progressive, spatio-temporal accumulation of A $\beta$ O in the hippocampus of 5xFAD mice (Figure 1b). A $\beta$ O first appear in the subiculum as early as 2 months of age (not shown), followed by continued accumulation in the subiculum and a spreading of pathology to CA1, CA2 and the dentate gyrus. This timing suggests that A $\beta$ O are associated with the observed memory loss.

396

#### ACU193 detects A $\beta$ O bound to primary neurons with high specificity

397

398

399

400

401

402

403

To validate the specificity of ACU193 for A $\beta$ O, the antibody was used *in vitro* to detect synthetic preparations of oligomers introduced into primary hippocampal neurons in culture (Supplemental Figure 1). Primary hippocampal neurons were treated with cross-linked A $\beta$ O, which have been shown to preserve A $\beta$ O structure *in vitro* (Cline et al., 2019b), or vehicle control. The cells were subsequently fixed and labeled with ACU193 at increasing dosages. Confocal imaging of the cells showed somatic staining of A $\beta$ O in addition to small, nanoscale puncta along dendritic processes (labeled with MAP2). These ACU193-positive puncta are likely A $\beta$ O binding to dendritic spines, as seen in previously published work

404 (Lacor et al., 2007; De Felice et al., 2009; Pitt et al., 2017). Minimal ACU193 labeling was observed on  
405 vehicle-treated neurons, indicating its specificity for A $\beta$ O.

### 406 **ACU193 and NU4 detect A $\beta$ O**

407 Additional support for the specificity of ACU193 can be seen in comparing the distribution of ACU193 in  
408 brain sections with the distribution of NU4, a well-established A $\beta$ O monoclonal antibody (Lambert et al.,  
409 2007; Xiao et al., 2013; Viola et al., 2015). Using ACU193 and NU4 conjugated to Alex Fluor 555 we  
410 found that both antibodies similarly detected A $\beta$ O in the subiculum and other areas of the hippocampus  
411 (Figure 2) including CA1, CA2 and the dentate gyrus. ACU193- (cyan) and NU4-positive (magenta) cells  
412 were observed accumulating in a nearly identical pattern, from 3 months to nine months of age. ACU193  
413 and NU4 selectively detect A $\beta$ O in the 5xFAD mice with virtually no signal in WT mice.

### 414 **Other Alzheimer's-associated pathologies also show developmental regulation in the** 415 **5xFAD mouse model**

416 To determine whether other Alzheimer's related pathologies show developmental regulation or  
417 accumulation in the 5xFAD mouse model for AD in association with A $\beta$ O, we examined  
418 immunohistochemical patterns of glial fibrillary acidic protein (GFAP), activated microglia (Iba1), and  
419 phosphorylated tau (pTau). Immunolabeling for pTau yielded difficult to interpret results which varied  
420 amongst the different antibodies for the same epitope and often did not match the literature. Instead, we  
421 focused on the inflammatory pathways, stimulated by the strong interest in the involvement of  
422 inflammatory responses in AD, in particular a new and growing interest in astrocytes (Wang et al., 2021).  
423 Sagittal sections from 5xFAD mice, aged 3-9 months, or their WT littermates were immunolabeled with  
424 antibodies against GFAP and co-labeled with ACU193, then imaged by confocal microscopy. We found  
425 a marked spatiotemporal association of GFAP pathology with ACU193-positive A $\beta$ O in the 5xFAD mice.  
426 GFAP (Figure 3, magenta) pathology first appeared in the subiculum at 3 months of age concurrent with  
427 the first appearance of A $\beta$ O (cyan) in the subiculum and in close proximity to one another. As the mice  
428 aged, GFAP and ACU193-positive pathology concomitantly spread throughout the subiculum and  
429 hippocampus (Figure 3, B & E). At 9 months, WT mice have minimal GFAP expression (Figure 3C) and  
430 no A $\beta$ O (Figure 3F). These patterns are consistent with possible induction of reactive astrogliosis by  
431 A $\beta$ O. At higher magnification, we observed GFAP-positive reactive astrocytes surrounding an ACU193-  
432 positive neuron and projecting their processes onto the cell soma (Figure 3I). In addition, we observed  
433 micron-wide ACU193-positive puncta adjacent to astrocytic processes distant from the cell soma.  
434 Immunolabeling for activated microglia (Iba1) (data not shown) indicated that the WT mice have more  
435 ramified microglial cells (resting) while 5xFAD littermates have more amoeboid and activated-shaped  
436 microglial cells. Microglial activation was evident at 2 months, with some increase in abundance seen in  
437 older animals.

### 438 **A $\beta$ O given to WT littermates induces memory impairment within 24 hours**

#### 439 ICV A $\beta$ O induce impairment in NLR/NOR

440 While the previous data indicate a relationship between A $\beta$ O accumulation and memory dysfunction in  
441 the 5xFAD mice, the question remained whether A $\beta$ O cause the observed memory loss. We therefore  
442 asked whether injection of A $\beta$ O into WT littermate mice would induce similar behavioral dysfunction.  
443 Wild-type littermates from the 5xFAD colony were injected with 10pmol synthetic A $\beta$ O, or vehicle control  
444 into the right lateral ventricle, following our previously established protocol (Cline et al., 2019b). After 24  
445 hours, the mice were assessed by the NLR task, and later, the NOR assay at 48 hours post-injection.  
446 We found that ICV injection of A $\beta$ O induce memory dysfunction within 24 hours and impacts both cortical  
447 (NOR) and hippocampal (NLR) memory (Figure 4). As in the 5xFAD mice, A $\beta$ O injected mice showed no  
448 preference to either new or old objects and explored both equally. Vehicle-injected mice scored no  
449 different from wild-type in these tasks. These data show that A $\beta$ O are sufficient to induce memory

450 impairment within 24 hours post-injection in wild-type mice. We next sought to establish the functional  
451 effect of neutralizing these A $\beta$ O in the 5xFAD mice.

## 452 **Oligomer-selective antibodies engage and neutralize A $\beta$ O responsible for memory** 453 **dysfunction in 5xFAD mice**

### 454 ACU193-based probes ameliorate memory dysfunction

455 We have previously observed no short-term detrimental impact after inoculation of our A $\beta$ O antibodies  
456 into 5xFAD mice, but no studies have been done to determine the long-term positive or negative effects  
457 in these mice. To determine the impact of A $\beta$ O-neutralization in 5xFAD mice, 6- and 7-month-old mice  
458 were first assessed for memory impairment using the NLR/NOR assay. Mice were then inoculated with  
459 ACU193-based probes and imaged 24 hours later *in vivo* to ensure target engagement (see next section).  
460 The mice were then housed for 30-40 days to monitor any adverse effects or changes in behavior before  
461 being reassessed for memory impairment in the NLR/NOR tasks. Strikingly, we found that 6-month-old  
462 5xFAD mice inoculated with the ACU193-based MRI probe had reversal of memory dysfunction, with  
463 performance the same as WT controls in the NOR task 30 days post-inoculation (Figure 5). The NLR  
464 assay showed the same restoration of memory (not shown). The ACUPET probe similarly ameliorated  
465 memory impairment, measured 40 days post-injection. As a control, 5xFAD mice injected with a human  
466 IgGPET probe showed no memory improvement (data not shown). Results show that the A $\beta$ O-selective  
467 ACU193 antibody engages A $\beta$ O *in vivo*, completely reversing memory dysfunction in the 5xFAD mice  
468 with no evidence of pathological side effects. The data establish A $\beta$ O as the primary instigators of  
469 cognitive dysfunction in 5xFAD mice and support the therapeutic relevance of A $\beta$ O-selective probes.

## 470 **A $\beta$ O imaged *in vivo* using ACU193-based probes distinguish 5xFAD from wild-type** 471 **mice**

### 472 MRI signal from ACUMNS distinguishes 5xFAD from wild-type mice.

473 Our previous work showed that A $\beta$ O can be detected *in vivo* in the 5xFAD mouse model using antibody-  
474 based MRI probes which were conjugated to magnetic nanostructures (MNS) (Viola et al., 2015). These  
475 prior studies used NU4 as the A $\beta$ O-targeting antibody, which as shown above, binds similarly to ACU193.  
476 Here we show that ACU193 can also be developed into a molecular probe for A $\beta$ O detection *in vivo*.  
477 After baseline imaging by MRI, 12-month-old mice were intranasally inoculated with MNS-conjugated  
478 ACU193 and allowed to recover overnight (about 16 hours) before imaging again (Figure 6). MRI data  
479 shows an accumulation of the ACUMNS probe in the hippocampus and cortex of the 5xFAD mice that is  
480 absent in WT controls. ImageJ quantification of signal intensity in the hippocampi of inoculated mice  
481 shows a ~ 30-fold increase in 5xFAD mice over their WT littermates. Using the ACUMNS probe in 18-  
482 month-old mice showed similarly robust AD-dependent MRI signal in the hippocampus of the 5xFAD  
483 animals, but signals obtained in younger animals (6-months old) were less consistent. These data add to  
484 previous studies with the NU4 probe and show that non-invasive *in vivo* imaging of A $\beta$ O is possible  
485 using the ACUMNS probe, suggesting its potential diagnostic value and ability to confirm target  
486 engagement

### 487 Development of an ACU193-based PET imaging probe for early A $\beta$ O detection.

488 While the spatial resolution of MRI is excellent, its sensitivity is lower than other imaging modalities such  
489 as positron emission tomography (PET). Given PET sensitivity is at least 100 times greater than MRI, we  
490 thought it might detect very low levels of A $\beta$ O during early stages of AD development. ACU193 was  
491 conjugated to DOTA, a chelator, as the initial step in the PET probe development. To ensure that this  
492 conjugation did not interfere with the antibody's ability to target A $\beta$ O, sagittal brain slices from 5xFAD  
493 mice were probed with the ACU193-DOTA probe and counterstained with Thioflavin S (ThioS) for amyloid  
494 plaques (Supplemental Figure 2). Results show that ACU193-DOTA detected A $\beta$ O in the 5xFAD brain  
495 and did not co-localize with ThioS, consistent with previously obtained results showing that ACU193 does  
496 not bind amyloid plaques cores (Cline et al., 2019a).



497 ACUPET detects pathology in the brains of 4-month and older 5xFAD mice.

498 The next step was to determine if radiolabeled ACU193-DOTA (ACUPET) detects AD-related A $\beta$ O in  
499 the 5xFAD mouse brain at an early age. ACU193-DOTA was incubated with <sup>64</sup>Cu and free isotopes were  
500 removed prior to tail vein injection into mice of either 4 or 18 months old. Mice were then imaged at 1, 4,  
501 and 24 hours post-injection for ACUPET distribution. At 4 hours post-injection, ACUPET accumulation in  
502 the brain was detectable (not shown), but not robust. By 24 hours, accumulation of the ACUPET probe  
503 in the brains of the 5xFAD animals was evident in both the 4-month-old animals (Supplemental Figure  
504 3A) and the 18 month old animals (Supplemental Figure 3B-D). Animals at 6, 7, 8 and 12 months were  
505 also examined and similarly were able to distinguish 5xFAD from WT mice (data not shown).

506 **A $\beta$ O are specifically detected in vivo by NU4PET**

507 NU4-based PET probe development

508 Given the success of the NU4-based MRI probe (Viola et al., 2015), an NU4-based probe was  
509 synthesized for PET imaging. NU4 was conjugated to DOTA and tested to ensure that this conjugation  
510 did not interfere with the antibody's ability to target A $\beta$ O. Primary hippocampal neurons, pre-treated with  
511 fluorescently conjugated A $\beta$ O (FAM-A $\beta$ O) and were probed with NU4-DOTA (Supplemental Figure 4).  
512 Data show that nearly all FAM-A $\beta$ O (magenta) were also labeled with the NU4-DOTA probe  
513 (colocalization seen as dark blue) and no free NU4-DOTA (cyan) was detected. Vehicle treated cells  
514 showed no NU4-DOTA binding. Data confirm the specificity of the NU4-DOTA probe for A $\beta$ O, necessary  
515 for its use for *in vivo* imaging.

516 NU4PET detects AD-related pathology *in vivo* in 5xFAD mice, distinguishing them from WT

517 Validation of the A $\beta$ O-PET probes as effective for early AD diagnostics requires verification that they  
518 produce an *in vivo* signal that depends on the presence of A $\beta$ O. To validate our new probe, NU4  
519 (Lambert et al., 2007; Acton et al., 2010) and non-specific IgG antibodies were conjugated to DOTA and  
520 then radiolabeled with positron emitter <sup>64</sup>Cu using Wipke and Wang's method (Wipke et al., 2002). Our  
521 next step was to image for A $\beta$ O by PET following probe delivery. Animals (12 total), 7 months of age,  
522 were injected via tail vein with either NU4PET or IgGPET and then imaged at T=1, 2, 4, 8, 20, 30, 40,  
523 and 44 hours after injection. After 44 hours, the animals were euthanized and their brains removed for a  
524 final *ex vivo* image of all 12 brains simultaneously (3 animals per group). Results showed the NU4PET  
525 specifically identified 5xFAD animals (Figure 7). No signal was detected in all three control groups (5xFAD  
526 with IgGPET; WT with NU4PET; WT with IgGPET).

527 The fraction of NU4PET probe retained (Supplemental Figure 5) showed good uptake into the brains of  
528 the 5xFAD mice but not the WT littermates (quantification of uptake; see Methods). For all mice, the  
529 IgGPET probe showed negligible signal. Quantification showed uptake into the brain was comparable to  
530 levels of uptake seen with the commercially available Pittsburgh Compound B (PiB) tracer (Mathis et al.,  
531 2003; Klunk et al., 2004). To corroborate the presence of A $\beta$ O in the animals used for these studies, we  
532 analyzed the brain tissue with immunofluorescence. After final PET imaging, the brains were fixed and  
533 stored in 10% sucrose until no longer radioactive. Brains were then sliced sagittally at 50  $\mu$ m and probed  
534 with ACU193. Images were collected and analyzed for ACU193 signal intensity (Supplemental Figure 6).  
535 Data showed that only 5xFAD mice, and not WT littermates, had A $\beta$ O pathology. Results confirm the  
536 NU4 PET probe gives a signal selective for A $\beta$ O-positive mice.

537

538

## DISCUSSION

539 Alzheimer's disease is costly and marked by accumulation of pathological hallmarks such as amyloid  
540 plaques and neuronal tangles of hyperphosphorylated tau. Because A $\beta$  plaques have shown poor  
541 correlation with AD progression, there has been a rise in the exploration and development of therapeutics  
542 that are not based on amyloid (Cummings et al., 2021). This shift in focus has resulted in numerous  
543 potential therapies that have made it into clinical trials, but so far there have been limitations on the impact  
544 of these potential therapies. As an alternative, focusing on A $\beta$ O as the target for diagnostics and  
545 therapeutics appears to be a promising strategy for developing disease modifying treatments and early  
546 diagnosis. Here, we confirm that A $\beta$ O can induce memory dysfunction in wild type mice and that A $\beta$ O  
547 build up in 5xFAD mice in a manner concomitant with astrocyte pathology and with memory dysfunction.  
548 Importantly, targeting this buildup with A $\beta$ O-selective antibodies rescues memory performance.  
549 Furthermore, we demonstrate that antibody-based brain imaging probes that target A $\beta$ O can be used  
550 to identify animals that present with AD pathology, indicating the value of A $\beta$ O-selective antibodies both  
551 for diagnostics and therapeutics.

552 Recent interest in inflammatory processes and their involvement in AD has grown. Our data showed a  
553 striking association between GFAP-positive astrocytes and ACU193-positive A $\beta$ O. This association and  
554 concomitant increase indicates a potential mechanism for A $\beta$ O-induced behavioral abnormalities. These  
555 findings are particularly intriguing given recent studies indicating AD's dependence on astrocytes. One  
556 especially interesting study showed that when apolipoprotein E (ApoE), a protein expressed in astrocytes  
557 which A $\beta$ O associate with at synapses, was knocked out in astrocyte-only populations of P301S mice,  
558 AD pathology markedly improved (Wang et al., 2021). As ApoE4 is the greatest genetic risk factor of late  
559 onset AD, we propose that it may mediate A $\beta$ O-induced reactive astrogliosis and the subsequent  
560 neuropathology instigated by reactive astrocytes. Another study showed that astrocytes were activated  
561 into their reactive state via the JAK/STAT3 pathway in 6 month-old 5xFAD mice (Choi et al., 2020).  
562 Consistent with the idea that reactive astrogliosis is necessary for behavioral dysfunction in 5xFAD mice,  
563 STAT3 phosphorylation inhibition restored cognitive function in the 5xFAD mice. Taken together with our  
564 data, we propose that A $\beta$ O may induce JAK/STAT3 pathway-dependent reactive astrogliosis in  
565 astrocytes which is necessary for observed cognitive dysfunction in 5xFAD mice. In addition to  
566 astrocytes, microglia play a major role in AD pathology. The Triggering Receptor Expressed on Myeloid  
567 cells 2 (TREM2)- expressed in microglia- has already been shown to be involved in AD, with mutations  
568 being neuroprotective and TREM2 accumulation being detected in AD patients (Jiang et al., 2013;  
569 Benitez et al., 2014; Guven et al., 2020). Previous studies have shown that A $\beta$ O associate with TREM2  
570 (Zhao et al., 2018; Zhong et al., 2019; Price et al., 2020), but TREM2 has no impact on established  
571 pathology (Yuan et al., 2021).

572 While interest increases in alternatives to the Amyloid Hypothesis, we are still left with no effective  
573 diagnostic tools for identifying AD at its earliest stages when therapeutics have the greatest impact.  
574 Currently recommended tests may rule out other dementia etiologies and help to determine disease  
575 severity, but they cannot detect AD at its earliest stages or closely predict disease progression as they  
576 do not probe for AD's earliest biomarkers. While AD diagnosis has significantly improved with the  
577 incorporation of a multiple assay evaluation currently being recommended, the tests still cannot predict  
578 disease progression or diagnose AD at its earliest stages because they are not quantifying the earliest  
579 biomarkers of the disease. However, alternative detection assays are being developed. Pre-tangle Tau,  
580 thought to be the toxic form of tau, has now been detected in MCI and AD and has been found to be one  
581 of the earliest tau lesions that correlates with cognitive status (Mufson et al., 2014). Synapse loss (Bastin  
582 et al., 2020; Buchanan et al., 2020; Camporesi et al., 2020; Mecca et al., 2020; Pereira et al., 2021),  
583 changes in hormone levels (Cheng et al., 2021), changes in blood biomarker levels (Guzman-Martinez  
584 et al., 2019; Montoliu-Gaya et al., 2021), electroencephalogram (EEG) readings (Hulbert and Adeli, 2013;  
585 Siwek et al., 2015; Lin et al., 2021), retinal assays (Ashok et al., 2020; Mirzaei et al., 2020), and changes  
586 in specific protein levels (Buchanan et al., 2020; Colom-Cadena et al., 2020) are some of the myriad

587 assays being developed to try to detect AD earlier and predict when and if the change from mild cognitive  
588 impairment (MCI) to AD will occur (Zhang et al., 2021b). All of these new developments are focused  
589 towards enabling earlier therapeutic intervention when chances for success would be greatest.

590 A $\beta$ O<sub>s</sub> as a diagnostic resource are currently unavailable. Cerebrospinal fluid assays show promise  
591 (Georganopoulou et al., 2005; Toledo et al., 2013a; Savage et al., 2014; Yang et al., 2015; Yang et al.,  
592 2019), but spinal taps are invasive and assays using CSF analytes have presented challenges with  
593 respect to accuracy and reliable disease-state discrimination (Slemmon et al., 2012). Other assays for  
594 A $\beta$ O levels are under development and show promise as well (Meng et al., 2019). For example, A $\beta$ O  
595 quantification in blood plasma shows a correlation between A $\beta$ O levels and declining memory scores that  
596 appear to not be influenced by age, gender, or ApoE4 status. Recently, the examination of soluble  
597 cortical extracts by ELISA found a link between the ratio of A $\beta$ O<sub>s</sub> and fibrils with disease. “The ratio of  
598 A $\beta$ O levels to plaque density fully distinguished demented from non-demented patients, with no overlap  
599 between groups in this derived variable.” (Esparza et al., 2013)

600 Because A $\beta$ O<sub>s</sub> are regarded as the first toxin to appear in disease progression, they should provide an  
601 excellent target for diagnostic imaging (Hefti et al., 2013; Goure et al., 2014). The usefulness of targeting  
602 A $\beta$ O<sub>s</sub> is indicated by human neuropathology studies in which A $\beta$ O<sub>s</sub> initially appear bound to discrete  
603 neurons, localizing to synapses in dendritic arbours (Lacor et al., 2004) through putative association with  
604 clustered cell surface receptors (Ferreira and Klein, 2011). FAM-A $\beta$ O<sub>s</sub> bind at discrete sites on dendrites,  
605 showing saturable, concentration-dependent synaptic binding (Viola et al., 2015), further suggesting their  
606 potential as a suitable target for an antibody-based diagnostic probe. Pronucleon™ imaging used  
607 engineered peptides that deliver a readout when associated with beta-rich A $\beta$  fibers and oligomeric A $\beta$   
608 (Nyborg et al., 2013). Several PET probes have also been developed including a probe from curcumin<sup>18</sup>F  
609 (Rokka et al., 2014), a probe created by modifying 6E10 antibody with PEG and <sup>64</sup>Cu that distinguished  
610 Tg from control mice (McLean et al., 2012), and a probe developed from an <sup>124</sup>I-labeled mAb158 against  
611 A $\beta$  protofibrils (Magnusson et al., 2013). Still, none of these probes specifically target A $\beta$ O<sub>s</sub>.

612 Previously, we described a molecular MRI probe that is targeted against A $\beta$ O<sub>s</sub> (Viola et al., 2015). Based  
613 on the success of our initial MRI probe and the antibody-based probes being explored by others, it is  
614 reasonable to predict that A $\beta$ O-specific antibodies can be used to target probes and provide better signal-  
615 to-noise ratios. Here we showed that anti-A $\beta$ O antibodies can be used to develop molecular MRI and PET  
616 probes that distinguish WT mice from their 5xFAD littermates at ages as early as 4 months old. These  
617 probes have proven to be non-toxic over the periods examined and, in fact, showed *in vivo* efficacy.

618 Early diagnostics are critical to combating this devastating disease, but without effective therapeutics,  
619 they have limited value. The first FDA-approved drug to treat Alzheimer’s disease (AD) in nearly two  
620 decades, Aduhelm®, shows a preferential affinity for all aggregated forms of amyloid beta (A $\beta$ ), rather  
621 than targeting only the toxic A $\beta$ O<sub>s</sub>. Currently, there are more than 126 agents in clinical trials, with most  
622 aimed at disease modification (Cummings, 2021; Cummings et al., 2021). While less than 10% of these  
623 target A $\beta$ , there remains evidence that A $\beta$  is a significant target for therapeutic development. Lowering  
624 A $\beta$ O levels by enhancing fibril formation has been shown to be protective (Mucke et al., 2000). This is  
625 supported by previous antibody-based studies (Lambert et al., 2007; Xiao et al., 2013). The data  
626 presented here importantly show that A $\beta$ O-selective antibodies rescue memory performance in a widely  
627 used AD model. These antibodies, which have been modified for use in brain imaging of A $\beta$ O, show great  
628 promise as potential agents for AD therapeutics and diagnostics; the potential of one A $\beta$ O-selective  
629 antibody is now being assessed in a recently begun clinical trial.

630

631

## 632 **Acknowledgements**

633 We would like to thank Samuel C. Bartley, Elizabeth A. Johnson, Matthew Perkins, Jake Vitrofsky, Alex  
634 L. Qin, Henry Weiss, Rohan Chalasani, and Erika N. Cline for their assistance that helped make this

635 study possible. We would like to thank the Northwestern University Research Experiences for  
636 Undergraduates program for their support.

637 This work was supported in part by NIH grants (R41AG054337, R21AG045637 to WLK and  
638 RF1AG063903 to Kelleher, Patrie, and WLK).

639 Microscopy was performed at the Biological Imaging Facility at Northwestern University  
640 (RRID:SCR\_017767), graciously supported by the Chemistry for Life Processes Institute, the NU Office  
641 for Research, the Department of Molecular Biosciences and the Rice Foundation\*\*.

642 MRI and PET/CT imaging work was performed at the Northwestern University Center for Advanced  
643 Molecular, graciously supported by the Chemistry for Life Processes Institute, the NU Office for  
644 Research. Imaging generously supported by NCI CCSG P30 CA060553 awarded to the Robert H Lurie  
645 Comprehensive Cancer Center.

646 Imaging work was performed at the Northwestern University High-Throughput Analysis Lab, graciously  
647 supported by the Chemistry for Life Processes Institute, the NU Office for Research.

648

649

650

## Contribution to the field statement

651  
652  
653  
654  
655  
656  
657  
658  
659  
660  
661  
662  
663  
664

Alzheimer's disease is costly and marked by pathological damage and progressive memory loss. While there has been progress made towards developing better therapeutics and diagnostics, it has been limited. Diagnostic improvements have primarily been in the development of better imaging methods, mostly using agents that probe amyloid fibrils and plaques- species that do not correlate well with disease progression and are not present at the earliest stages of the disease. Amyloid  $\beta$  oligomers (A $\beta$ O) are now widely accepted as the A $\beta$  species most germane to AD onset and progression. Here we report evidence further supporting the role of A $\beta$ O in Alzheimer's disease and introduce a promising anti-A $\beta$ O diagnostic probe capable of distinguishing the 5xFAD mouse model from wild type mice by PET and MRI. Our studies also showed a concomitant development of memory impairment with the accumulation of A $\beta$ O and reactive astrocytes. Compelling support for the conclusion that A $\beta$ O cause memory loss was found in experiments showing that A $\beta$ O-selective antibodies into 5xFAD mice completely restored memory function. These antibodies, modified to give imaging probes, were able to distinguish 5xFAD mice from wild type littermates. These results demonstrate that A $\beta$ O selective antibodies have potential both for therapeutics and for diagnostics.



665

## References

- 666 (2021). 2021 Alzheimer's disease facts and figures. *Alzheimers Dement* 17(3), 327-406. doi:  
667 10.1002/alz.12328.
- 668 Acton, P.Q., PA, US), An, Z.A., PA, US), Bett, A.J.L., PA, US), Breese, R.Q., PA, US), Chang,  
669 L.W., IL, US), Dodson, E.C.S., PA, US), et al. (2010). *Anti-ADDL antibodies and uses*  
670 *thereof*. United States patent application 11/256332. 08/24/2010.
- 671 Albert, M.S., DeKosky, S.T., Dickson, D., Dubois, B., Feldman, H.H., Fox, N.C., et al. (2011).  
672 The diagnosis of mild cognitive impairment due to Alzheimer's disease: recommendations  
673 from the National Institute on Aging-Alzheimer's Association workgroups on diagnostic  
674 guidelines for Alzheimer's disease. *Alzheimers Dement* 7(3), 270-279. doi:  
675 10.1016/j.jalz.2011.03.008.
- 676 Antunes, M., and Biala, G. (2012). The novel object recognition memory: neurobiology, test  
677 procedure, and its modifications. *Cogn Process* 13(2), 93-110. doi: 10.1007/s10339-011-  
678 0430-z.
- 679 Ashe, K.H. (2020). The biogenesis and biology of amyloid beta oligomers in the brain.  
680 *Alzheimers Dement* 16(11), 1561-1567. doi: 10.1002/alz.12084.
- 681 Ashok, A., Singh, N., Chaudhary, S., Bellamkonda, V., Kritikos, A.E., Wise, A.S., et al. (2020).  
682 Retinal Degeneration and Alzheimer's Disease: An Evolving Link. *Int J Mol Sci* 21(19).  
683 doi: 10.3390/ijms21197290.
- 684 Bastin, C., Bahri, M.A., Meyer, F., Manard, M., Delhaye, E., Plenevaux, A., et al. (2020). In vivo  
685 imaging of synaptic loss in Alzheimer's disease with [18F]UCB-H positron emission  
686 tomography. *Eur J Nucl Med Mol Imaging* 47(2), 390-402. doi: 10.1007/s00259-019-  
687 04461-x.
- 688 Bengoetxea, X., Rodriguez-Perdigon, M., and Ramirez, M.J. (2015). Object recognition test for  
689 studying cognitive impairments in animal models of Alzheimer's disease. *Front Biosci*  
690 *(Schol Ed)* 7, 10-29.
- 691 Benitez, B.A., Jin, S.C., Guerreiro, R., Graham, R., Lord, J., Harold, D., et al. (2014). Missense  
692 variant in TREML2 protects against Alzheimer's disease. *Neurobiol Aging* 35(6),  
693 1510.e1519-1526. doi: 10.1016/j.neurobiolaging.2013.12.010.
- 694 Bicca, M.A., Costa, R., Loch-Neckel, G., Figueiredo, C.P., Medeiros, R., and Calixto, J.B. (2015).  
695 B(2) receptor blockage prevents Abeta-induced cognitive impairment by  
696 neuroinflammation inhibition. *Behav Brain Res* 278, 482-491. doi:  
697 10.1016/j.bbr.2014.10.040.
- 698 Braak, H., and Del Tredici, K. (2011). Alzheimer's pathogenesis: is there neuron-to-neuron  
699 propagation? *Acta Neuropathol* 121(5), 589-595. doi: 10.1007/s00401-011-0825-z.
- 700 Buchanan, H., Mackay, M., Palmer, K., Tothová, K., Katsur, M., Platt, B., et al. (2020). Synaptic  
701 Loss, ER Stress and Neuro-Inflammation Emerge Late in the Lateral Temporal Cortex  
702 and Associate with Progressive Tau Pathology in Alzheimer's Disease. *Mol Neurobiol*  
703 57(8), 3258-3272. doi: 10.1007/s12035-020-01950-1.
- 704 Camporesi, E., Nilsson, J., Brinkmalm, A., Becker, B., Ashton, N.J., Blennow, K., et al. (2020).  
705 Fluid Biomarkers for Synaptic Dysfunction and Loss. *Biomark Insights* 15,  
706 1177271920950319. doi: 10.1177/1177271920950319.
- 707 Chang, L., Bakhos, L., Wang, Z., Venton, D.L., and Klein, W.L. (2003). Femtomole  
708 immunodetection of synthetic and endogenous amyloid-beta oligomers and its application  
709 to Alzheimer's disease drug candidate screening. *J Mol Neurosci* 20(3), 305-313. doi:  
710 10.1385/JMN:20:3:305.

- 711 Cheng, Y.J., Lin, C.H., and Lane, H.Y. (2021). From Menopause to Neurodegeneration-  
712 Molecular Basis and Potential Therapy. *Int J Mol Sci* 22(16). doi: 10.3390/ijms22168654.
- 713 Choi, M., Kim, H., Yang, E.J., and Kim, H.S. (2020). Inhibition of STAT3 phosphorylation  
714 attenuates impairments in learning and memory in 5XFAD mice, an animal model of  
715 Alzheimer's disease. *J Pharmacol Sci* 143(4), 290-299. doi: 10.1016/j.jphs.2020.05.009.
- 716 Cline, E., Viola, K., Klein, W., Wang, X., Bacskai, B., Rammes, G., et al. (2019a). "Synaptic  
717 intervention in Alzheimer's disease: soluble A $\beta$  oligomer directed ACU193 monoclonal  
718 antibody therapeutic for treatment of early Alzheimer's disease", in: *Clinical Trials on  
719 Alzheimer's disease*. (San Diego, CA, USA).
- 720 Cline, E.N., Bicca, M.A., Viola, K.L., and Klein, W.L. (2018). The Amyloid-beta Oligomer  
721 Hypothesis: Beginning of the Third Decade. *J Alzheimers Dis* 64(s1), S567-S610. doi:  
722 10.3233/JAD-179941.
- 723 Cline, E.N., Das, A., Bicca, M.A., Mohammad, S.N., Schachner, L.F., Kamel, J.M., et al. (2019b).  
724 A novel crosslinking protocol stabilizes amyloid beta oligomers capable of inducing  
725 Alzheimer's-associated pathologies. *J Neurochem* 148(6), 822-836. doi:  
726 10.1111/jnc.14647.
- 727 Cohen, S.J., and Stackman, R.W., Jr. (2015). Assessing rodent hippocampal involvement in the  
728 novel object recognition task. A review. *Behav Brain Res* 285, 105-117. doi:  
729 10.1016/j.bbr.2014.08.002.
- 730 Colom-Cadena, M., Spires-Jones, T., Zetterberg, H., Blennow, K., Caggiano, A., DeKosky, S.T.,  
731 et al. (2020). The clinical promise of biomarkers of synapse damage or loss in Alzheimer's  
732 disease. *Alzheimers Res Ther* 12(1), 21. doi: 10.1186/s13195-020-00588-4.
- 733 Cummings, J. (2021). Drug Development for Psychotropic, Cognitive-Enhancing, and Disease-  
734 Modifying Treatments for Alzheimer's Disease. *J Neuropsychiatry Clin Neurosci* 33(1), 3-  
735 13. doi: 10.1176/appi.neuropsych.20060152.
- 736 Cummings, J., Lee, G., Zhong, K., Fonseca, J., and Taghva, K. (2021). Alzheimer's disease drug  
737 development pipeline: 2021. *Alzheimers Dement (N Y)* 7(1), e12179. doi:  
738 10.1002/trc2.12179.
- 739 De Felice, F.G., Vieira, M.N., Bomfim, T.R., Decker, H., Velasco, P.T., Lambert, M.P., et al.  
740 (2009). Protection of synapses against Alzheimer's-linked toxins: insulin signaling  
741 prevents the pathogenic binding of A $\beta$  oligomers. *Proc Natl Acad Sci U S A* 106(6),  
742 1971-1976. doi: 10.1073/pnas.0809158106.
- 743 Denninger, J.K., Smith, B.M., and Kirby, E.D. (2018). Novel Object Recognition and Object  
744 Location Behavioral Testing in Mice on a Budget. *J Vis Exp* (141). doi: 10.3791/58593.
- 745 Devi, L., Alldred, M.J., Ginsberg, S.D., and Ohno, M. (2010). Sex- and brain region-specific  
746 acceleration of beta-amyloidogenesis following behavioral stress in a mouse model of  
747 Alzheimer's disease. *Mol Brain* 3, 34. doi: 10.1186/1756-6606-3-34.
- 748 Esparza, T.J., Zhao, H., Cirrito, J.R., Cairns, N.J., Bateman, R.J., Holtzman, D.M., et al. (2013).  
749 Amyloid-beta oligomerization in Alzheimer dementia versus high-pathology controls. *Ann  
750 Neurol* 73(1), 104-119. doi: 10.1002/ana.23748.
- 751 Ferreira, S.T., and Klein, W.L. (2011). The A $\beta$  oligomer hypothesis for synapse failure and  
752 memory loss in Alzheimer's disease. *Neurobiol Learn Mem* 96(4), 529-543. doi:  
753 10.1016/j.nlm.2011.08.003.
- 754 Gandy, S., Simon, A.J., Steele, J.W., Lublin, A.L., Lah, J.J., Walker, L.C., et al. (2010). Days to  
755 criterion as an indicator of toxicity associated with human Alzheimer amyloid-beta  
756 oligomers. *Ann Neurol* 68(2), 220-230. doi: 10.1002/ana.22052.

- 757 Georganopoulou, D.G., Chang, L., Nam, J.M., Thaxton, C.S., Mufson, E.J., Klein, W.L., et al.  
758 (2005). Nanoparticle-based detection in cerebral spinal fluid of a soluble pathogenic  
759 biomarker for Alzheimer's disease. *Proc Natl Acad Sci U S A* 102(7), 2273-2276. doi:  
760 10.1073/pnas.0409336102.
- 761 Girard, S.D., Baranger, K., Gauthier, C., Jacquet, M., Bernard, A., Escoffier, G., et al. (2013).  
762 Evidence for early cognitive impairment related to frontal cortex in the 5XFAD mouse  
763 model of Alzheimer's disease. *J Alzheimers Dis* 33(3), 781-796. doi: 10.3233/jad-2012-  
764 120982.
- 765 Girard, S.D., Jacquet, M., Baranger, K., Migliorati, M., Escoffier, G., Bernard, A., et al. (2014).  
766 Onset of hippocampus-dependent memory impairments in 5XFAD transgenic mouse  
767 model of Alzheimer's disease. *Hippocampus* 24(7), 762-772. doi: 10.1002/hipo.22267.
- 768 Gong, Y., Chang, L., Viola, K.L., Lacor, P.N., Lambert, M.P., Finch, C.E., et al. (2003).  
769 Alzheimer's disease-affected brain: presence of oligomeric A beta ligands (ADDLs)  
770 suggests a molecular basis for reversible memory loss. *Proc Natl Acad Sci U S A* 100(18),  
771 10417-10422. doi: 10.1073/pnas.1834302100.
- 772 Goure, W.F., Krafft, G.A., Jerecic, J., and Hefti, F. (2014). Targeting the proper amyloid-beta  
773 neuronal toxins: a path forward for Alzheimer's disease immunotherapeutics. *Alzheimers*  
774 *Res Ther* 6(4), 42. doi: 10.1186/alzrt272.
- 775 Grayson, B., Leger, M., Piercy, C., Adamson, L., Harte, M., and Neill, J.C. (2015). Assessment  
776 of disease-related cognitive impairments using the novel object recognition (NOR) task in  
777 rodents. *Behav Brain Res* 285, 176-193. doi: 10.1016/j.bbr.2014.10.025.
- 778 Guntern, R., Bouras, C., Hof, P.R., and Vallet, P.G. (1992). An improved thioflavine S method  
779 for staining neurofibrillary tangles and senile plaques in Alzheimer's disease. *Experientia*  
780 48(1), 8-10. doi: 10.1007/BF01923594.
- 781 Guven, G., Bilgic, B., Samanci, B., Gurvit, H., Hanagasi, H., Donmez, C., et al. (2020). Peripheral  
782 TREM2 mRNA levels in early and late-onset Alzheimer disease's patients. *Mol Biol Rep*  
783 47(8), 5903-5909. doi: 10.1007/s11033-020-05661-7.
- 784 Guzman-Martinez, L., Maccioni, R.B., Farías, G.A., Fuentes, P., and Navarrete, L.P. (2019).  
785 Biomarkers for Alzheimer's Disease. *Curr Alzheimer Res* 16(6), 518-528. doi:  
786 10.2174/1567205016666190517121140.
- 787 Hampel, H., Hardy, J., Blennow, K., Chen, C., Perry, G., Kim, S.H., et al. (2021). The Amyloid-  
788 beta Pathway in Alzheimer's Disease. *Mol Psychiatry*. doi: 10.1038/s41380-021-01249-  
789 0.
- 790 Hefti, F., Goure, W.F., Jerecic, J., Iverson, K.S., Walicke, P.A., and Krafft, G.A. (2013). The case  
791 for soluble Abeta oligomers as a drug target in Alzheimer's disease. *Trends Pharmacol*  
792 *Sci* 34(5), 261-266. doi: 10.1016/j.tips.2013.03.002.
- 793 Hsia, A.Y., Masliah, E., McConlogue, L., Yu, G.Q., Tatsuno, G., Hu, K., et al. (1999). Plaque-  
794 independent disruption of neural circuits in Alzheimer's disease mouse models. *Proc Natl*  
795 *Acad Sci U S A* 96(6), 3228-3233.
- 796 Hulbert, S., and Adeli, H. (2013). EEG/MEG- and imaging-based diagnosis of Alzheimer's  
797 disease. *Rev Neurosci* 24(6), 563-576. doi: 10.1515/revneuro-2013-0042.
- 798 Investor Relations, B. (2021). "FDA grants accelerated approval for ADUHELM™ as the first and  
799 only Alzheimer's disease treatment to address a defining pathology of the disease".  
800 ([www.biogen.com](http://www.biogen.com): Biogen).
- 801 Jack, C.R., Jr., Albert, M.S., Knopman, D.S., McKhann, G.M., Sperling, R.A., Carrillo, M.C., et  
802 al. (2011). Introduction to the recommendations from the National Institute on Aging-

- 803 Alzheimer's Association workgroups on diagnostic guidelines for Alzheimer's disease.  
804 *Alzheimers Dement* 7(3), 257-262. doi: 10.1016/j.jalz.2011.03.004.
- 805 Jawhar, S., Trawicka, A., Jenneckens, C., Bayer, T.A., and Wirths, O. (2012). Motor deficits,  
806 neuron loss, and reduced anxiety coinciding with axonal degeneration and intraneuronal  
807 Abeta aggregation in the 5XFAD mouse model of Alzheimer's disease. *Neurobiol Aging*  
808 33(1), 196 e129-140. doi: 10.1016/j.neurobiolaging.2010.05.027.
- 809 Jiang, T., Yu, J.T., Zhu, X.C., and Tan, L. (2013). TREM2 in Alzheimer's disease. *Mol Neurobiol*  
810 48(1), 180-185. doi: 10.1007/s12035-013-8424-8.
- 811 Johnson, K.A., Minoshima, S., Bohnen, N.I., Donohoe, K.J., Foster, N.L., Herscovitch, P., et al.  
812 (2013). Appropriate use criteria for amyloid PET: a report of the Amyloid Imaging Task  
813 Force, the Society of Nuclear Medicine and Molecular Imaging, and the Alzheimer's  
814 Association. *Alzheimers Dement* 9(1), e-1-16. doi: 10.1016/j.jalz.2013.01.002.
- 815 Kanno, T., Tsuchiya, A., and Nishizaki, T. (2014). Hyperphosphorylation of Tau at Ser396 occurs  
816 in the much earlier stage than appearance of learning and memory disorders in 5XFAD  
817 mice. *Behav Brain Res* 274, 302-306. doi: 10.1016/j.bbr.2014.08.034.
- 818 Kaye, R., Head, E., Thompson, J.L., McIntire, T.M., Milton, S.C., Cotman, C.W., et al. (2003).  
819 Common structure of soluble amyloid oligomers implies common mechanism of  
820 pathogenesis. *Science* 300(5618), 486-489. doi: 10.1126/science.1079469.
- 821 Kimura, R., and Ohno, M. (2009). Impairments in remote memory stabilization precede  
822 hippocampal synaptic and cognitive failures in 5XFAD Alzheimer mouse model. *Neurobiol*  
823 *Dis* 33(2), 229-235. doi: 10.1016/j.nbd.2008.10.006.
- 824 Klunk, W.E., Engler, H., Nordberg, A., Wang, Y., Blomqvist, G., Holt, D.P., et al. (2004). Imaging  
825 brain amyloid in Alzheimer's disease with Pittsburgh Compound-B. *Ann Neurol* 55(3),  
826 306-319. doi: 10.1002/ana.20009.
- 827 Krafft, G., Hefti, F., Goure, W., Jerecic, J., Iverson, K., and Walicke, P. (2013). ACU-193: A  
828 candidate therapeutic antibody that selectively targets soluble beta-amyloid oligomers.  
829 *Alzheimer's & Dementia* 9(4, Supplement), P326. doi:  
830 <http://dx.doi.org/10.1016/j.jalz.2013.04.166>.
- 831 Lacor, P.N., Buniel, M.C., Chang, L., Fernandez, S.J., Gong, Y., Viola, K.L., et al. (2004).  
832 Synaptic targeting by Alzheimer's-related amyloid beta oligomers. *J Neurosci* 24(45),  
833 10191-10200. doi: 10.1523/JNEUROSCI.3432-04.2004.
- 834 Lacor, P.N., Buniel, M.C., Furlow, P.W., Clemente, A.S., Velasco, P.T., Wood, M., et al. (2007).  
835 Abeta oligomer-induced aberrations in synapse composition, shape, and density provide  
836 a molecular basis for loss of connectivity in Alzheimer's disease. *J Neurosci* 27(4), 796-  
837 807. doi: 10.1523/JNEUROSCI.3501-06.2007.
- 838 Lambert, M.P., Barlow, A.K., Chromy, B.A., Edwards, C., Freed, R., Liosatos, M., et al. (1998).  
839 Diffusible, nonfibrillar ligands derived from Abeta1-42 are potent central nervous system  
840 neurotoxins. *Proc Natl Acad Sci U S A* 95(11), 6448-6453.
- 841 Lambert, M.P., Velasco, P.T., Chang, L., Viola, K.L., Fernandez, S., Lacor, P.N., et al. (2007).  
842 Monoclonal antibodies that target pathological assemblies of Abeta. *J Neurochem* 100(1),  
843 23-35. doi: 10.1111/j.1471-4159.2006.04157.x.
- 844 Lasagna-Reeves, C.A., Castillo-Carranza, D.L., Sengupta, U., Guerrero-Munoz, M.J., Kiritoshi,  
845 T., Neugebauer, V., et al. (2012). Alzheimer brain-derived tau oligomers propagate  
846 pathology from endogenous tau. *Sci Rep* 2, 700. doi: 10.1038/srep00700.
- 847 Lee, S.P., Falangola, M.F., Nixon, R.A., Duff, K., and Helpert, J.A. (2004). Visualization of beta-  
848 amyloid plaques in a transgenic mouse model of Alzheimer's disease using MR



- 849 microscopy without contrast reagents. *Magn Reson Med* 52(3), 538-544. doi:  
850 10.1002/mrm.20196.
- 851 Lesne, S., Koh, M.T., Kotilinek, L., Kaye, R., Glabe, C.G., Yang, A., et al. (2006). A specific  
852 amyloid-beta protein assembly in the brain impairs memory. *Nature* 440(7082), 352-357.  
853 doi: 10.1038/nature04533.
- 854 Li, S., and Selkoe, D.J. (2020). A mechanistic hypothesis for the impairment of synaptic plasticity  
855 by soluble Abeta oligomers from Alzheimer's brain. *J Neurochem* 154(6), 583-597. doi:  
856 10.1111/jnc.15007.
- 857 Lin, N., Gao, J., Mao, C., Sun, H., Lu, Q., and Cui, L. (2021). Differences in Multimodal  
858 Electroencephalogram and Clinical Correlations Between Early-Onset Alzheimer's  
859 Disease and Frontotemporal Dementia. *Front Neurosci* 15, 687053. doi:  
860 10.3389/fnins.2021.687053.
- 861 Magnusson, K., Sehlin, D., Syvanen, S., Svedberg, M.M., Philipson, O., Soderberg, L., et al.  
862 (2013). Specific uptake of an amyloid-beta protofibril-binding antibody-tracer in AbetaPP  
863 transgenic mouse brain. *J Alzheimers Dis* 37(1), 29-40. doi: 10.3233/jad-130029.
- 864 Masters, C.L., Simms, G., Weinman, N.A., Multhaup, G., McDonald, B.L., and Beyreuther, K.  
865 (1985). Amyloid plaque core protein in Alzheimer disease and Down syndrome. *Proc Natl*  
866 *Acad Sci U S A* 82(12), 4245-4249.
- 867 Mathis, C.A., Wang, Y., Holt, D.P., Huang, G.F., Debnath, M.L., and Klunk, W.E. (2003).  
868 Synthesis and evaluation of <sup>11</sup>C-labeled 6-substituted 2-arylbenzothiazoles as amyloid  
869 imaging agents. *J Med Chem* 46(13), 2740-2754. doi: 10.1021/jm030026b.
- 870 McKhann, G.M., Knopman, D.S., Chertkow, H., Hyman, B.T., Jack, C.R., Jr., Kawas, C.H., et al.  
871 (2011). The diagnosis of dementia due to Alzheimer's disease: recommendations from  
872 the National Institute on Aging-Alzheimer's Association workgroups on diagnostic  
873 guidelines for Alzheimer's disease. *Alzheimers Dement* 7(3), 263-269. doi:  
874 10.1016/j.jalz.2011.03.005.
- 875 McLean, D., Cooke, M.J., Wang, Y., Green, D., Fraser, P.E., George-Hyslop, P.S., et al. (2012).  
876 Anti-amyloid-beta-mediated positron emission tomography imaging in Alzheimer's  
877 disease mouse brains. *PLoS One* 7(12), e51958. doi: 10.1371/journal.pone.0051958.
- 878 Mecca, A.P., Chen, M.K., O'Dell, R.S., Naganawa, M., Toyonaga, T., Godek, T.A., et al. (2020).  
879 In vivo measurement of widespread synaptic loss in Alzheimer's disease with SV2A PET.  
880 *Alzheimers Dement* 16(7), 974-982. doi: 10.1002/alz.12097.
- 881 Meng, X., Li, T., Wang, X., Lv, X., Sun, Z., Zhang, J., et al. (2019). Association between  
882 increased levels of amyloid- $\beta$  oligomers in plasma and episodic memory loss in  
883 Alzheimer's disease. *Alzheimer's Research & Therapy* 11(1), 89. doi: 10.1186/s13195-  
884 019-0535-7.
- 885 Mirzaei, N., Shi, H., Oviatt, M., Doustar, J., Rentsendorj, A., Fuchs, D.T., et al. (2020).  
886 Alzheimer's Retinopathy: Seeing Disease in the Eyes. *Front Neurosci* 14, 921. doi:  
887 10.3389/fnins.2020.00921.
- 888 Montoliu-Gaya, L., Strydom, A., Blennow, K., Zetterberg, H., and Ashton, N.J. (2021). Blood  
889 Biomarkers for Alzheimer's Disease in Down Syndrome. *J Clin Med* 10(16). doi:  
890 10.3390/jcm10163639.
- 891 Mucke, L., Masliah, E., Yu, G.Q., Mallory, M., Rockenstein, E.M., Tatsuno, G., et al. (2000).  
892 High-level neuronal expression of abeta 1-42 in wild-type human amyloid protein  
893 precursor transgenic mice: synaptotoxicity without plaque formation. *Journal of*  
894 *Neuroscience* 20(11), 4050-4058.



- 895 Mucke, L., and Selkoe, D.J. (2012). Neurotoxicity of amyloid beta-protein: synaptic and network  
896 dysfunction. *Cold Spring Harb Perspect Med* 2(7), a006338. doi:  
897 10.1101/cshperspect.a006338.
- 898 Mufson, E.J., Ward, S., and Binder, L. (2014). Prefibrillar tau oligomers in mild cognitive  
899 impairment and Alzheimer's disease. *Neurodegener Dis* 13(2-3), 151-153. doi:  
900 10.1159/000353687.
- 901 Mundt, A.P., Winter, C., Mueller, S., Wuerfel, J., Tysiak, E., Schnorr, J., et al. (2009). Targeting  
902 activated microglia in Alzheimer's pathology by intraventricular delivery of a  
903 phagocytosable MRI contrast agent in APP23 transgenic mice. *Neuroimage* 46(2), 367-  
904 372. doi: 10.1016/j.neuroimage.2009.01.067.
- 905 Nandwana, V., Ryoo, S.-R., Kanthala, S., De, M., Chou, S.S., Prasad, P.V., et al. (2016).  
906 Engineered Theranostic Magnetic Nanostructures: Role of Composition and Surface  
907 Coating on Magnetic Resonance Imaging Contrast and Thermal Activation. *ACS Applied*  
908 *Materials & Interfaces* 8(11), 6953-6961. doi: 10.1021/acsami.6b01377.
- 909 Nyborg, A.C., Moll, J.R., Wegrzyn, R.D., Havas, D., Hutter-Paier, B., Feuerstein, G.G., et al.  
910 (2013). In vivo and ex vivo imaging of amyloid-beta cascade aggregates with a  
911 Pronucleon peptide. *J Alzheimers Dis* 34(4), 957-967. doi: 10.3233/jad-122107.
- 912 Oakley, H., Cole, S.L., Logan, S., Maus, E., Shao, P., Craft, J., et al. (2006). Intraneuronal beta-  
913 amyloid aggregates, neurodegeneration, and neuron loss in transgenic mice with five  
914 familial Alzheimer's disease mutations: potential factors in amyloid plaque formation. *J*  
915 *Neurosci* 26(40), 10129-10140. doi: 10.1523/JNEUROSCI.1202-06.2006.
- 916 Oblak, A.L., Lin, P.B., Kotredes, K.P., Pandey, R.S., Garceau, D., Williams, H.M., et al. (2021).  
917 Comprehensive Evaluation of the 5XFAD Mouse Model for Preclinical Testing  
918 Applications: A MODEL-AD Study. *Front Aging Neurosci* 13, 713726. doi:  
919 10.3389/fnagi.2021.713726.
- 920 Ohno, M. (2009). Failures to reconsolidate memory in a mouse model of Alzheimer's disease.  
921 *Neurobiol Learn Mem* 92(3), 455-459. doi: 10.1016/j.nlm.2009.05.001.
- 922 Ohno, M., Chang, L., Tseng, W., Oakley, H., Citron, M., Klein, W.L., et al. (2006). Temporal  
923 memory deficits in Alzheimer's mouse models: rescue by genetic deletion of BACE1. *Eur*  
924 *J Neurosci* 23(1), 251-260. doi: 10.1111/j.1460-9568.2005.04551.x.
- 925 Ou-Yang, M.H., and Van Nostrand, W.E. (2013). The absence of myelin basic protein promotes  
926 neuroinflammation and reduces amyloid beta-protein accumulation in Tg-5xFAD mice. *J*  
927 *Neuroinflammation* 10, 134. doi: 10.1186/1742-2094-10-134.
- 928 Overk, C.R., and Masliah, E. (2014). Toward a unified therapeutics approach targeting putative  
929 amyloid-beta oligomer receptors. *Proc Natl Acad Sci U S A* 111(38), 13680-13681. doi:  
930 10.1073/pnas.1414554111.
- 931 Park, S.Y., Avraham, H.K., and Avraham, S. (2004). RAFTK/Pyk2 activation is mediated by  
932 trans-acting autophosphorylation in a Src-independent manner. *J Biol Chem* 279(32),  
933 33315-33322. doi: 10.1074/jbc.M313527200.
- 934 Pereira, J.B., Janelidze, S., Ossenkoppele, R., Kivitsberg, H., Brinkmalm, A., Mattsson-  
935 Carlgren, N., et al. (2021). Untangling the association of amyloid- $\beta$  and tau with synaptic  
936 and axonal loss in Alzheimer's disease. *Brain* 144(1), 310-324. doi:  
937 10.1093/brain/awaa395.
- 938 Pitt, J., Wilcox, K.C., Tortelli, V., Diniz, L.P., Oliveira, M.S., Dobbins, C., et al. (2017).  
939 Neuroprotective astrocyte-derived insulin/insulin-like growth factor 1 stimulates endocytic

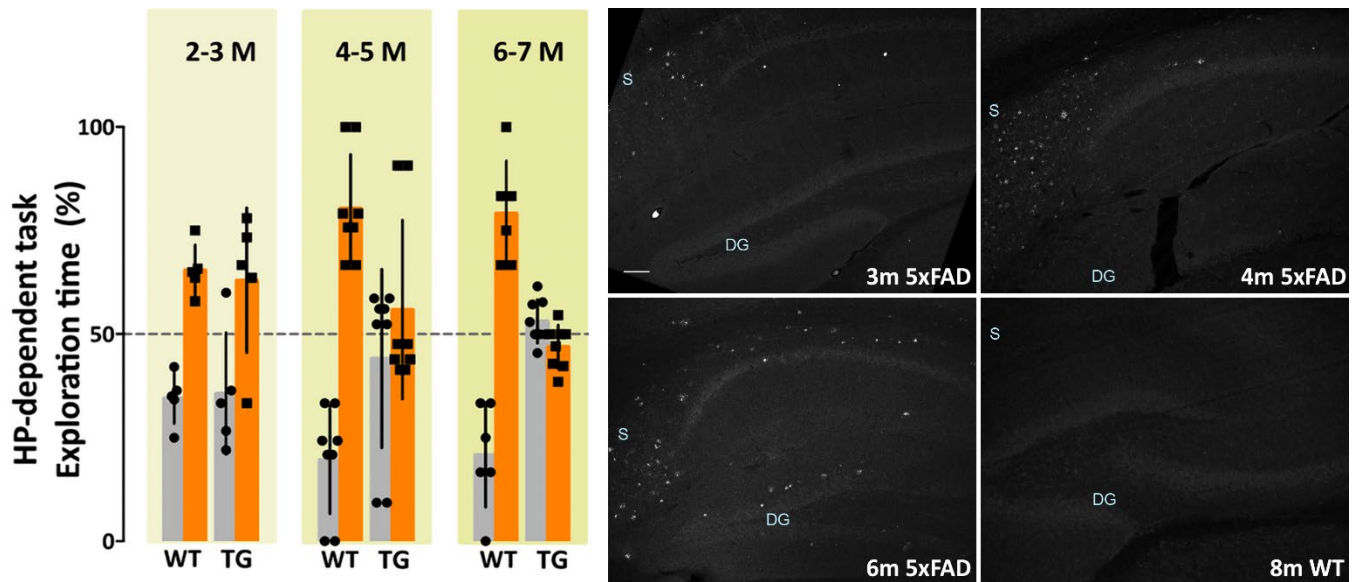
- 940 processing and extracellular release of neuron-bound Abeta oligomers. *Mol Biol Cell*  
941 28(20), 2623-2636. doi: 10.1091/mbc.E17-06-0416.
- 942 Price, B.R., Sudduth, T.L., Weekman, E.M., Johnson, S., Hawthorne, D., Woolums, A., et al.  
943 (2020). Therapeutic Trem2 activation ameliorates amyloid-beta deposition and improves  
944 cognition in the 5XFAD model of amyloid deposition. *J Neuroinflammation* 17(1), 238. doi:  
945 10.1186/s12974-020-01915-0.
- 946 Robakis, N.K. (2011). Mechanisms of AD neurodegeneration may be independent of Abeta and  
947 its derivatives. *Neurobiol Aging* 32(3), 372-379. doi:  
948 10.1016/j.neurobiolaging.2010.05.022.
- 949 Rodgers, A.B. (2005). "Progress report on Alzheimer's disease 2004-2005". U.S.Department of  
950 Health and Human Services; National Institutes on Aging; National Institutes of Health).
- 951 Rokka, J., Snellman, A., Zona, C., La Ferla, B., Nicotra, F., Salmona, M., et al. (2014). Synthesis  
952 and evaluation of a (18)F-curcumin derivate for beta-amyloid plaque imaging. *Bioorg Med*  
953 *Chem* 22(9), 2753-2762. doi: 10.1016/j.bmc.2014.03.010.
- 954 Savage, M.J., Kalinina, J., Wolfe, A., Tugusheva, K., Korn, R., Cash-Mason, T., et al. (2014). A  
955 sensitive abeta oligomer assay discriminates Alzheimer's and aged control cerebrospinal  
956 fluid. *J Neurosci* 34(8), 2884-2897. doi: 10.1523/jneurosci.1675-13.2014.
- 957 Schnabel, J. (2011). Amyloid: little proteins, big clues. *Nature* 475(7355), S12-14. doi:  
958 10.1038/475S12a.
- 959 Selkoe, D.J., and Hardy, J. (2016). The amyloid hypothesis of Alzheimer's disease at 25 years.  
960 *EMBO Mol Med* 8(6), 595-608. doi: 10.15252/emmm.201606210.
- 961 Shao, C.Y., Mirra, S.S., Sait, H.B., Sacktor, T.C., and Sigurdsson, E.M. (2011). Postsynaptic  
962 degeneration as revealed by PSD-95 reduction occurs after advanced Abeta and tau  
963 pathology in transgenic mouse models of Alzheimer's disease. *Acta Neuropathol* 122(3),  
964 285-292. doi: 10.1007/s00401-011-0843-x.
- 965 Siwek, M.E., Muller, R., Henseler, C., Trog, A., Lundt, A., Wormuth, C., et al. (2015). Altered  
966 Theta Oscillations and Aberrant Cortical Excitatory Activity in the 5XFAD Model of  
967 Alzheimer's Disease. *Neural Plast* 2015, 781731. doi: 10.1155/2015/781731.
- 968 Slemmon, J.R., Meredith, J., Guss, V., Andreasson, U., Andreasen, N., Zetterberg, H., et al.  
969 (2012). Measurement of Abeta1-42 in cerebrospinal fluid is influenced by matrix effects.  
970 *J Neurochem* 120(2), 325-333. doi: 10.1111/j.1471-4159.2011.07553.x.
- 971 Sperling, R.A., Aisen, P.S., Beckett, L.A., Bennett, D.A., Craft, S., Fagan, A.M., et al. (2011).  
972 Toward defining the preclinical stages of Alzheimer's disease: recommendations from the  
973 National Institute on Aging-Alzheimer's Association workgroups on diagnostic guidelines  
974 for Alzheimer's disease. *Alzheimers Dement* 7(3), 280-292. doi:  
975 10.1016/j.jalz.2011.03.003.
- 976 Terry, R.D., Masliah, E., Salmon, D.P., Butters, N., DeTeresa, R., Hill, R., et al. (1991). Physical  
977 basis of cognitive alterations in Alzheimer's disease: synapse loss is the major correlate  
978 of cognitive impairment. *Ann Neurol* 30(4), 572-580. doi: 10.1002/ana.410300410.
- 979 Toledo, J.B., Korff, A., Shaw, L.M., Trojanowski, J.Q., and Zhang, J. (2013a). CSF alpha-  
980 synuclein improves diagnostic and prognostic performance of CSF tau and Abeta in  
981 Alzheimer's disease. *Acta Neuropathol* 126(5), 683-697. doi: 10.1007/s00401-013-1148-  
982 z.
- 983 Toledo, J.B., Xie, S.X., Trojanowski, J.Q., and Shaw, L.M. (2013b). Longitudinal change in CSF  
984 Tau and Abeta biomarkers for up to 48 months in ADNI. *Acta Neuropathol* 126(5), 659-  
985 670. doi: 10.1007/s00401-013-1151-4.

- 986 Townsend, M., Shankar, G.M., Mehta, T., Walsh, D.M., and Selkoe, D.J. (2006). Effects of  
987 secreted oligomers of amyloid beta-protein on hippocampal synaptic plasticity: a potent  
988 role for trimers. *J Physiol* 572(Pt 2), 477-492. doi: 10.1113/jphysiol.2005.103754.
- 989 Viola, K.L., and Klein, W.L. (2015). Amyloid beta oligomers in Alzheimer's disease pathogenesis,  
990 treatment, and diagnosis. *Acta Neuropathol* 129(2), 183-206. doi: 10.1007/s00401-015-  
991 1386-3.
- 992 Viola, K.L., Sbarboro, J., Sureka, R., De, M., Bicca, M.A., Wang, J., et al. (2015). Towards non-  
993 invasive diagnostic imaging of early-stage Alzheimer's disease. *Nat Nanotechnol* 10(1),  
994 91-98. doi: 10.1038/nnano.2014.254.
- 995 Wang, C., Xiong, M., Gratuze, M., Bao, X., Shi, Y., Andhey, P.S., et al. (2021). Selective removal  
996 of astrocytic APOE4 strongly protects against tau-mediated neurodegeneration and  
997 decreases synaptic phagocytosis by microglia. *Neuron* 109(10), 1657-1674 e1657. doi:  
998 10.1016/j.neuron.2021.03.024.
- 999 Wang, H.W., Pasternak, J.F., Kuo, H., Ristic, H., Lambert, M.P., Chromy, B., et al. (2002).  
1000 Soluble oligomers of beta amyloid (1-42) inhibit long-term potentiation but not long-term  
1001 depression in rat dentate gyrus. *Brain Res* 924(2), 133-140.
- 1002 Wipke, B.T., Wang, Z., Kim, J., McCarthy, T.J., and Allen, P.M. (2002). Dynamic visualization of  
1003 a joint-specific autoimmune response through positron emission tomography. *Nat*  
1004 *Immunol* 3(4), 366-372. doi: 10.1038/ni775.
- 1005 Xiao, C., Davis, F.J., Chauhan, B.C., Viola, K.L., Lacor, P.N., Velasco, P.T., et al. (2013). Brain  
1006 transit and ameliorative effects of intranasally delivered anti-amyloid-beta oligomer  
1007 antibody in 5XFAD mice. *J Alzheimers Dis* 35(4), 777-788. doi: 10.3233/JAD-122419.
- 1008 Yang, T., Dang, Y., Ostaszewski, B., Mengel, D., Steffen, V., Rabe, C., et al. (2019). Target  
1009 engagement in an alzheimer trial: Crenezumab lowers amyloid beta oligomers in  
1010 cerebrospinal fluid. *Ann Neurol* 86(2), 215-224. doi: 10.1002/ana.25513.
- 1011 Yang, Y., Kim, J., Kim, H.Y., Ryoo, N., Lee, S., Kim, Y., et al. (2015). Amyloid-beta Oligomers  
1012 May Impair SNARE-Mediated Exocytosis by Direct Binding to Syntaxin 1a. *Cell Rep*  
1013 12(8), 1244-1251. doi: 10.1016/j.celrep.2015.07.044.
- 1014 Yuan, Q., Liu, X., Zhang, Y., Xian, Y.F., Zou, J., Zhang, X., et al. (2021). Established Beta  
1015 Amyloid Pathology Is Unaffected by TREM2 Elevation in Reactive Microglia in an  
1016 Alzheimer's Disease Mouse Model. *Molecules* 26(9). doi: 10.3390/molecules26092685.
- 1017 Zhang, M., Zhong, L., Han, X., Xiong, G., Xu, D., Zhang, S., et al. (2021a). Brain and Retinal  
1018 Abnormalities in the 5xFAD Mouse Model of Alzheimer's Disease at Early Stages. *Front*  
1019 *Neurosci* 15, 681831. doi: 10.3389/fnins.2021.681831.
- 1020 Zhang, T., Liao, Q., Zhang, D., Zhang, C., Yan, J., Ngetich, R., et al. (2021b). Predicting MCI to  
1021 AD Conversion Using Integrated sMRI and rs-fMRI: Machine Learning and Graph  
1022 Theory Approach. *Front Aging Neurosci* 13, 688926. doi: 10.3389/fnagi.2021.688926.
- 1023 Zhao, Y., Wu, X., Li, X., Jiang, L.L., Gui, X., Liu, Y., et al. (2018). TREM2 Is a Receptor for  $\beta$ -  
1024 Amyloid that Mediates Microglial Function. *Neuron* 97(5), 1023-1031.e1027. doi:  
1025 10.1016/j.neuron.2018.01.031.
- 1026 Zhong, L., Xu, Y., Zhuo, R., Wang, T., Wang, K., Huang, R., et al. (2019). Soluble TREM2  
1027 ameliorates pathological phenotypes by modulating microglial functions in an Alzheimer's  
1028 disease model. *Nat Commun* 10(1), 1365. doi: 10.1038/s41467-019-09118-9.

1029  
1030

1031

## Figures, Titles, and Legends



1032

1033

**Figure 1**

1034

1035

1036

1037

1038

1039

1040

1041

1042

1043

1044

1045

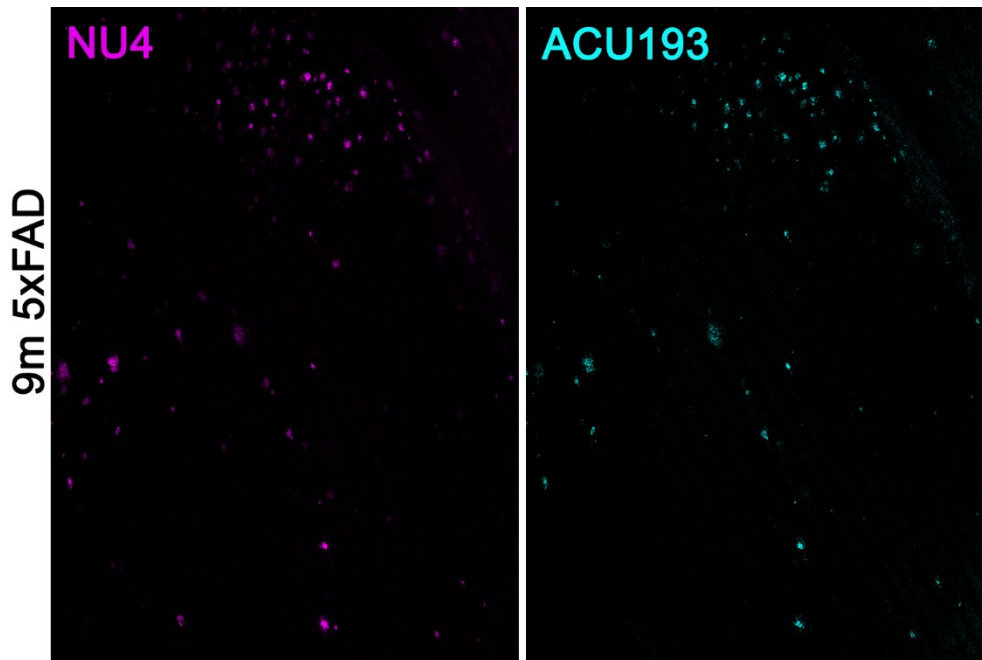
1046

1047

1048

**Memory dysfunction in 5xFAD mice is substantial by 4 months and is preceded by A $\beta$ O pathology, detectable by 3 months of age.** (Left) 5xFAD mice and wild-type littermates were assessed for memory dysfunction using novel location recognition (NLR; hippocampal-dependent task) and novel object recognition tasks (NOR; cortical-dependent task). Ages ranged 2-12 months. Data shown here are for the hippocampal-dependent NLR assay (similar results with NOR, not shown). In 5xFAD mice, memory impairment was negligible at 2-3 months, substantial by 4-5 months, and fully penetrant by 6 months of age. Statistical analysis shows that there was no significant difference between the behaviors of the WT mice and the 5xFAD mice at ages 2-3 months, but a statistically significant difference was evident between the recognition task behaviors of the WT mice and 5xFAD mice for ages 4-5 months ( $p < 0.001$ ) and 6-7 months ( $p < 0.0001$ ). (Right) Sagittal brain sections were obtained from 5xFAD and WT mice at ages 2, 3, 4, 6, and 8 months and probed for A $\beta$ O pathology using a humanized A $\beta$ O monoclonal antibody. Fluorescent signal was barely detectable at 2 months of age (not shown), was more readily detectable by 3 months, and robust by 6 months. Wild-type littermates presented no signal. Scale bar = 100  $\mu$ m.





1049

1050

**Figure 2**

1051

1052

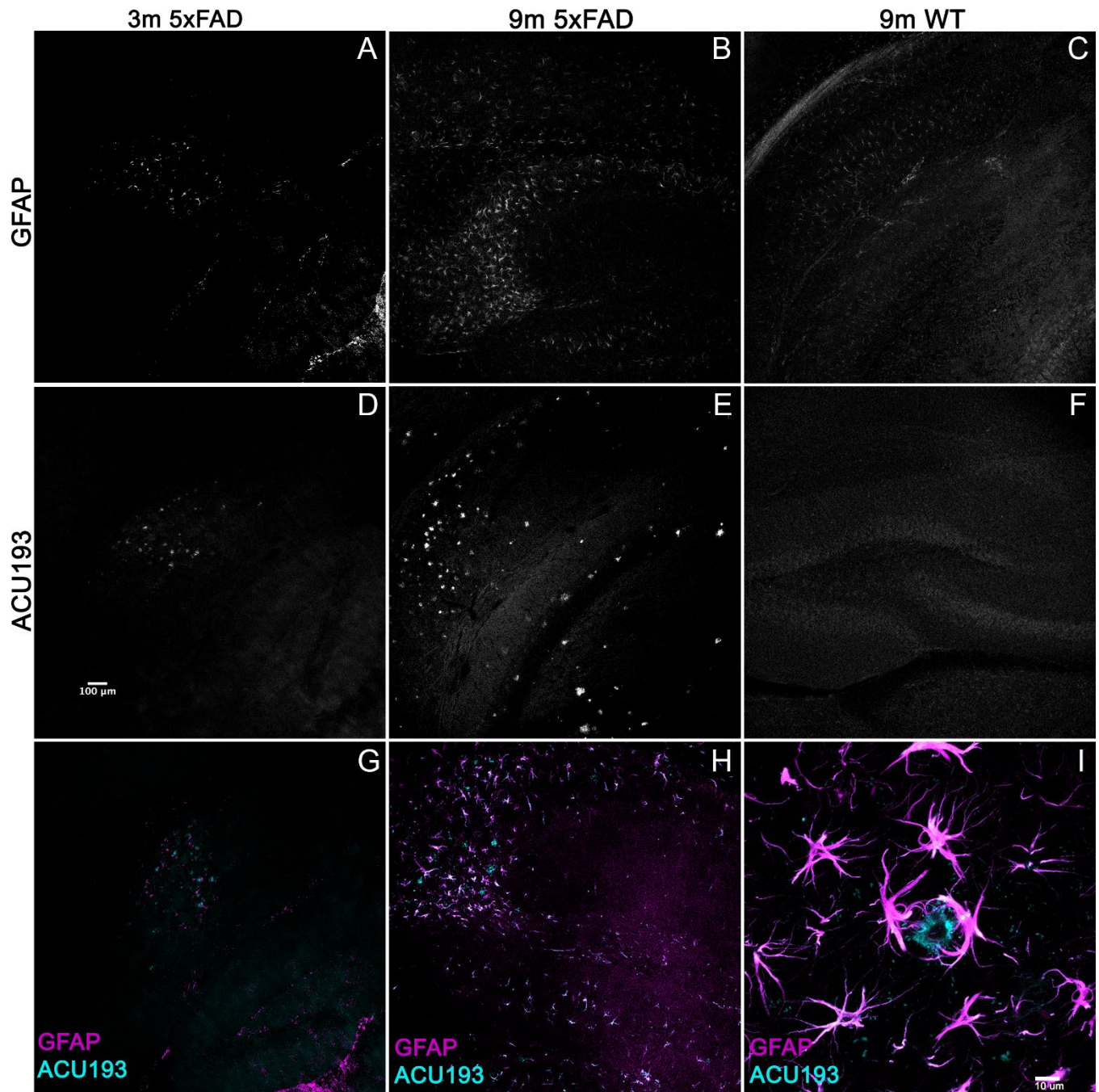
1053

1054

1055

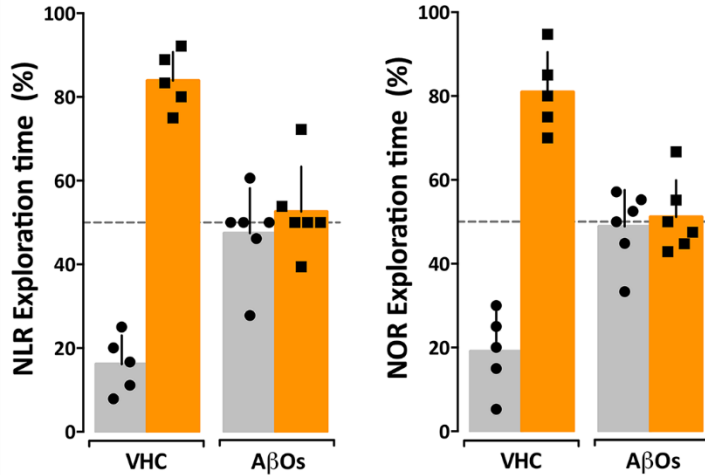
**ACU193 and NU4 detect AβOs ex vivo.** Sagittal sections from 9-month-old 5xFAD mice were immunolabeled with 2 different anti-AβO antibodies, NU4 and ACU193, to determine the extent to which AβO pathology is detected by both antibodies. Data show that AβOs accumulate and that ACU193 and NU4 show very similar detection of AβOs.





1056  
1057 **Figure 3**

1058 **GFAP is activated in a developmental manner in the 5xFAD mouse.** Sagittal sections from 5xFAD  
1059 mice, aged 3-9 months, and their wild-type littermates were immunolabeled with antibodies against  
1060 GFAP and ACU193, then imaged on the Leica SP5 confocal microscope at 10x and 100x. Data show  
1061 that, like the ACU193, GFAP positive glial cells accumulate in an age dependent manner. Sale bar =  
1062 100 µm for panels A-H ad 10 µm for panel I.

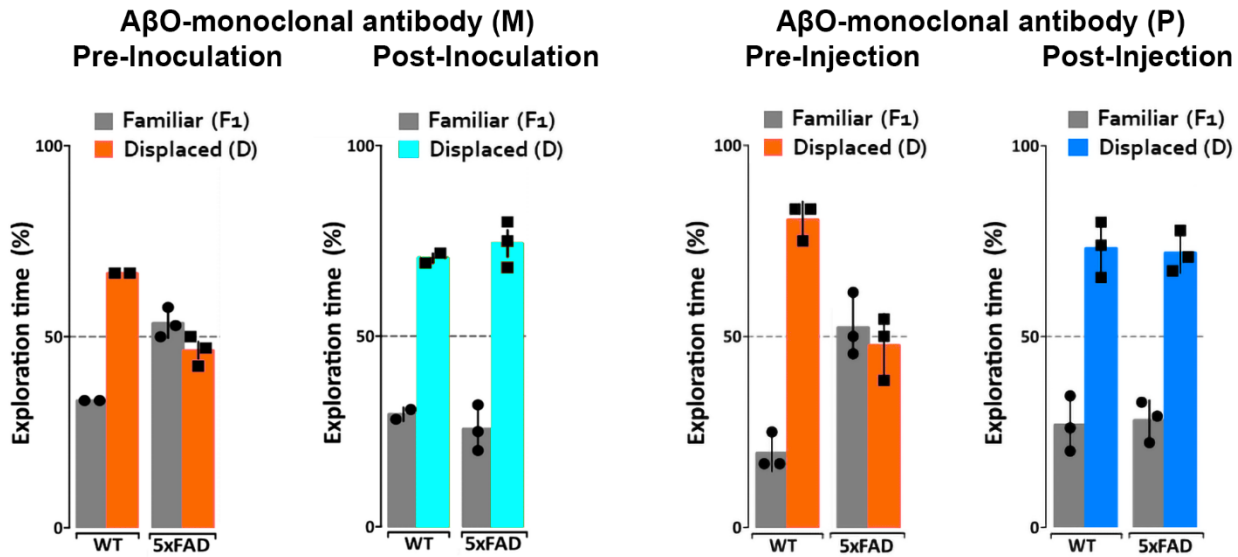


1064

1065

#### Figure 4

1066 **Intraventricular AβO injection caused memory impairment in wild type mice within 24 hours.** Wild  
1067 type mice were tested for performance in recognition tasks beginning 24 hours after receiving AβO  
1068 injections (10 pmols in 3 μl) into the right lateral ventricle. Mice first were assessed for novel location  
1069 recognition (NLR; 24 hr post-injection) and subsequently for novel object recognition (NOR; 48 hr post-  
1070 injection). AβO-injected mice were unable to perform either recognition task. Statistical analysis shows  
1071 that there is a statistically significant difference between the recognition task behaviors of the WT mice  
1072 and the AβO injected mice ( $p < 0.0001$ ).  
1073



1074

1075

**Figure 5**

1076

**ACUMNS delivered intranasally and ACUPET given iv both rescue memory function in 6- to 7-month-old mice.**

1077

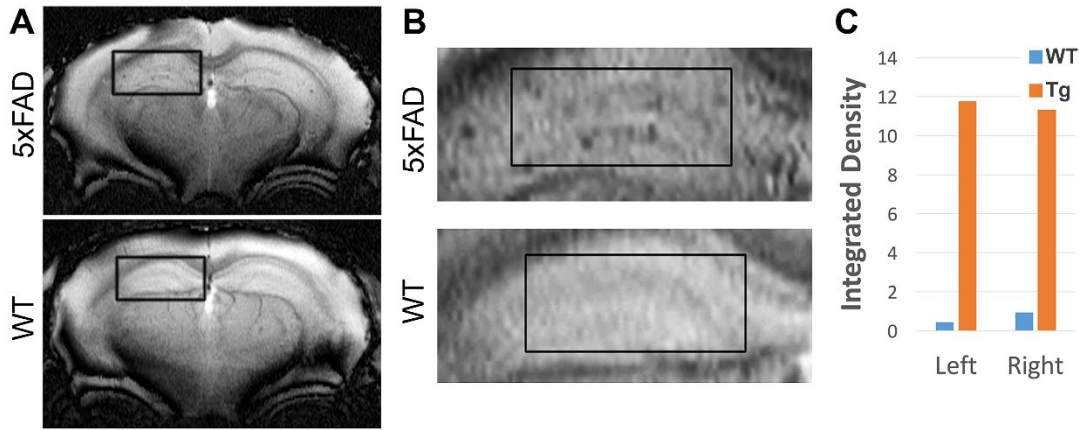
1078

Tg and WT mice, aged 6 and 18 months (Left set of bar graphs), were tested by NLR and NOR assays to ensure predicted behavioral deficits. Mice were then intranasally inoculated with ACUMNS and imaged for probe distribution and detection of AβO pathology *in vivo*. After imaging, animals were monitored for 30 days for signs of adverse reactions to the probe (none detected), then re-tested by NOR. The 6-month-old animals showed a significant recovery of memory impairment 30 days after inoculation. This recovery was not observed in the very old animals, although some memory improvement was seen (data not shown). To test the impact of the ACUPET probe on memory function, Tg and WT mice, aged 7 months, were tested by NLR and NOR assays prior to imaging as before. Mice were then injected, via tail vein, with ACUPET or non-specific IgGPET and imaged for up to 24 hours to monitor probe distribution. After imaging, animals were monitored for 40 days for signs of adverse reactions to the probe. Animals were re-tested by NOR at 40 days recovery. 5xFAD animals injected with ACUPET showed a persistent recovery of memory impairment that was not seen in the 5xFAD animals injected with IgGPET. Data support the long-term benefits of these antibody-based probes on memory.

1089

1090

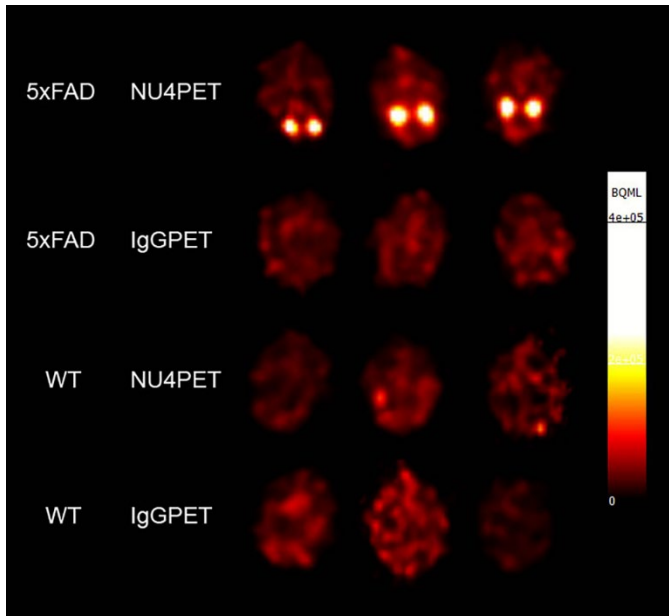
1091



1092  
1093 **Figure 6**

1094 **ACUMNS gives AD-dependent MRI signal in hippocampus of 12-month-old 5xFAD mice.**

1095 *In vivo* studies with ACUMNS probe show robust AD-dependent MRI signal in the hippocampus of 12  
1096 month-old mice.  
1097



1098

1099

### Figure 7

**NU4PET probe gives 5xFAD- specific CNS signal that is maintained even 44 hr after iv injection.**

Signal obtained after IV injection of NU4PET showed probe accumulation in the hippocampus of 5xFAD mice (aged 5-7 months). Controls (IgGPET in AD mice; NU4PET in wild type littermates; IgGPET in wild type littermates) showed no signal (3 animals per group).

1104